UNIVERSITY OF BELGRADE

SCHOOL OF ELECTRICAL ENGENNERING

Giuma Saleh Isa Abudagel

Experimental Characterization of Magneto-Optical Properties of Faraday Crystal Applied in Magnetic Field Sensor

Doctoral Dissertation

Belgrade, 2018

UNIVERZITET U BEOGRADU

ELEKTROTEHNIČKI FAKULTET

Giuma Saleh Isa Abudagel

Eksperimentalna karakterizacija magneto-optičkih osobina Faradejevog kristala namenjenog za konstrukciju senzora magnetskog polja

doktorska disertacija

Beograd 2018.

Mentor of Doctoral Dissertation

Associate prof. Dr. Slobodan Petricevic
University of Belgrade, School of Electrical Engineering

Members of Committee:

Full prof. dr Zlatan Stojković
University of Belgrade, School of Electrical Engineering

Dr Nebojša Romčević, scientific adviser
University of Belgrade, Institute of Physics, Belgrade

Associate prof. dr Peđa Mihailović
University of Belgrade, School of Electrical Engineering

Assistant prof. dr Marko Barjaktarović
University of Belgrade, School of Electrical Engineering

Defense date: _____

Acknowledgements

Dissertation Title: Experimental Characterization of Magneto-Optical Properties of Faraday Crystal Applied in Magnetic Field Sensor

Abstract: The thesis explores preparation and magneto properties of bismuth germanium oxide single crystal ($B_{12}GeO_{20}$) which is irradiated by pulsed femtosecond laser of increasing power. Analyses performed on irradiated and un irradiated samples showed significant changes in transmittance, transmission spectra, sample color, Raman spectra (RS), X-ray diffraction (XRD) pattern, Verdet constant (VC), magneto-optical property and absorption coefficient. After irradiation, the transmission spectra values increased whereas anisotropy detected in the transmission spectra of unirradiated samples disappeared. The change of color caused by irradiation was noticeable to the naked eye. The XRD measurements confirmed structural changes induced by laser irradiation, i.e., the laser- beam-incident side of the sample became almost amorphous, whereas the side opposite to the incident can be indexed to the Bi_{12} Ge O_{20} compound. Irradiation caused increase of Raman spectra peaks with the exception of crystal peaks of type E, which disappeared. The femtosecond pulsed laser irradiation can be used to improve bismuth germanium oxide single crystal optical properties. Femtosecond pulsed laser irradiation can improve optical properties of Bi_{12} GeO_{20} single crystals.

Keywords: Faraday crystal, magnetic field sensor, delta/sigma normalization, crystal temperature properties

Scientific field: Electrical Engineering

Scientific discipline: Optoelectronics

UDC: 621.3

Naslov teze: Eksperimentalna karakterizacija magneto-optičkih osobina Faradejevog kristala namenjenog za konstrukciju senzora magnetskog polja

Rezime: Disertacija razmatra pripremu za proizvodnju i magneto optička svojstva Bizmut germanijum oksidnih kristala ($B_{12}GeO_{20}$) koje se ozračuju femtosekundnim laserskim impulsima zracima sa rastućom snagom. Analize izvršene nad ozračenim i neozračenim uzorcima kristala pokazale su značajne promene u transmitansi, transmisionom spektru, boji, Ramanovom spektru, rezultatima difrakcije X zraka, Verdeovoj konstanti, magneto-optičkim svojstvima i koeficijentu apsorpcije. Posle ozračivanja došlo je do porasta transmitivnosti i izostanka anizotropije u transmisionom spektru u odnosu na neozračene uzorke. Izmena boje uzoraka primetna je čak i golim okom. XRD merenja pokazala su strukturne promene indukovane laserskim zracima tako da je npr. strana uzorka neposredno ozračena laserom postala skoro potpuno amorfna dok se suprotna strana uzorka indeksira na $B_{12}GeO_{20}$ jedinjenje. Ozračivanje je izazvalo porast vrhova u Ramanovom spektru sa izuzetkom vrhova za tip E koji se nisu pojavili. Femtosekundni laserski impulsi mogu se iskoristiti da unaprede optička svojstva kristala.

Ključne reči: Faradejev kristal, senzor magnetskog polja, delta/sigma normalizacija, temperaturska svojstva kristala

Naučna oblast: Elektrotehnika i računarstvo
Uža naučna oblast: Optoelektronika
UDC: 621.3

NOMENCLATURE

η_F	Faraday ellipticity
	dielectric tensor
$\frac{\Delta}{\varepsilon}$	difference-over-sum
γ	magneto gyration coefficient
λ	Wave Length
μ_0	permeability of free space
μ	permeability tensor
ω	frequency of the incident light
ω_k	resonance frequency
σ	conductivity tensor
ρ_0	electric charge density
φ	relative phase difference between the waves
θ	rotation angle of the polarization plane
a	Width of each coil
$\vec{B}$	magnetic flux density
$\vec{D}$	electric flux density
$\vec{E}$	electric field intensity
E_{0x}	amplitude of the waves in x direction
E_{0y}	amplitude of the waves in y direction
$\vec{H}$	magnetic field intensity
$\vec{J}$	electric current density
B	magnetic flux density
C	speed of light
d	Diameter of wire
f	frequency of light
H_k^{hf}	hyperfine coupling constants
I	Current
I_{max}	maximum current

f_k oscillator strengths

k extinction coefficient

K   propagation vector

L   path length

N   Number of turns per coil

$n_\pm$ refractive indices

P   rotatory power

V   Verdet constant

R   Distance between coils

r   radius of the coil

r_e classical electron radius

T   temperature

U_1 & U_2 voltages after trans impedance stage

Z   distance

ABBREVIATIONS

AC	Alternating Current
ADC	Analog to Digital Converter
BGO	Bismuth Germanium Oxide
CS	Current Source
DC	Direct Current
DSR	Distance to Spot Ratio
EDFA	Erbium Doped Fiber Amplifier
FE	Faraday Effect
FFT	Fast Fourier Transform
FIFO	First In, First Out
FOCS	Fiber Optic Current Sensor
FOV	Field of View
FR	Faraday Rotation
IF	Infra-red
HC	Helmholtz Coil
MAS	Measurement Acquisition System
MOE	Magneto Optical Effect
MOKE	Magneto Optical Kerr Effect
MOQ	Magneto Optical Quality
MP	Motorized Positioner
LCPL	Left Circularly Polarized Light
OA	Optical Activity
OI	Optical Isolator
POLP	Plane of Linearly Polarized
POP	Plane of Polarization
RCPL	Right Circularly Polarized Light
RS	Raman Spectra
SNR	Signal to Noise Ratio
QPD	Quadrant Photodiode
VC	Verdet Constant
XRD	X Ray Diffraction

Table of Contents

List of Figures

List of Tables

INTRODUCTION

Bismuth germanium oxide ($Bi_{12}GeO_{20}$) from the sillenite group of cubic crystals is commonly abbreviated as BGO or s-BGO. Due to its fitting optical characteristics, such as photoconductivity, photochromism, photorefractivity, piezoelectricity, as well as to electro-optic and magneto-optic effects it supports, it has been used in a wide range of optical applications and devices. Its cubic cell unit is composed of two formula units, namely of 24 Bi, 40 O and 2 Ge. The Ge atoms positioned in the center and the vertices of a cube are tetrahedrally coordinated by the oxygen atoms, whereas the Bi atoms are heptacoordinated. There are numerous studies that considered properties of doped and un-doped BGO, as well as those investigating property changes induced by a wide variety of exposure types such as thermal treatments, particle beams or light treatments. BGO is a good example of a Faraday rotator crystal possibly applicable in sensor systems. In order to evaluate usability of a crystal for sensing purposes not only its Faraday rotation capability, but its ability to be integrated into a sensing optical system must be considered. In general, in fiber-optic sensing systems optical beams used to sense the measured quantity are guided through the fibers, giving rise to the absorption coefficient as the most important optical property. Crystals with high absorption coefficient are in general less useful for sensor systems because they absorb much of the light and cause low signal-to-noise ratio at the receiving photo diode. Modulation of the light intensity caused by magnetic field rises with the Verdet constant increase, whereas the intensity of light reaching the photodiode, as well as the photocurrent, decrease with the crystal absorption increase. The noise in a fiber optic sensing system is predominantly determined by the noise in the processing electronics and can be expressed as the noise present in the photocurrent. Therefore, the signal-to-noise ratio of the magnetic field sensor rises with the Verdet constant increase, and declines with the crystal absorption increase. The magneto-optical quality of a crystal is defined as a ratio of the Faraday rotation, which is proportional to the Verdet constant, and the absorption coefficient. Consequently the magneto-

optical quality of a crystal can be used as a measure of a crystal's applicability in a magnetic field sensing system. When Bi12GeO20 crystals were exposed to pulsed laser beam irradiation, there are examples of laser beam operating in the nanosecond, picosecond , or femtosecond range [1]. In [1] it was determined that femtosecond pulsed laser irradiation of increasing power causes significant changes in the transmittance, transmission spectra, sample color, Raman spectra, X-ray diffraction pattern, Verdet constant, magneto-optical property, and absorption coefficient of lower quality black Bi12GeO20 single crystals. Here we analyze if the same increasing power pattern of femtosecond pulsed laser irradiation has similar effect on the high quality yellow $Bi_{12}GeO_{20}$ single crystals, i.e., on the crystals that were grown from the components whose purity is higher than that of the black crystals, and whose magneto-optical quality is the maximal obtainable by the applied crystal growth technique[2].

1. An Overview of the Research Efforts
1.1. Motivation Behind the Research

Faraday effect magnetic field sensors and current sensors (indirect, via magnetic field measurement) are an interesting non-conventional solution for measuring these quantities providing important advantages such as small size, excellent high voltage insulation, huge bandwidth, lower maintenance costs and others. Digitalization of power system networks and development of smart grids place new challenges on old methods and favors novel, optical means [3]. Single most important part of the Faraday Effect sensor is a volume of material (usually solid state material such as crystals) immersed in the magnetic field that causes the light passing through the volume to change its polarization parameters. Given the fact that some of these materials are insulators and thus do not perturb significantly the measured magnetic field their prospect is to replace conventional sensors, particularly those based on the transformer technology.

A typical Faraday sensor can be realized using optical fibers as light guides, since it is expensive to realize unfolded in-the-air sensor due to mounting complexity. Optical fiber provide means for relaxing mechanical requirements for mounts and can lead to more compact unit. However, employing fibers that do not change state of polarization or are not part of the polarimetric sensing, does not affect the model and operation of the sensor. Such configuration where fibers are only used to guide light into and from the sensing head are called extrinsic type sensor, and most conclusions in this thesis are actually valid for this type of sensor.

Motivation behind this research is centered on performance of the sensing element in the extrinsic type of Faraday sensor, since this configuration practical and a lot of research effort was invested in its development.

1.2.   Some Aspects of Faraday Magnetic Field and Current Sensors

Traditional Faraday sensing is polarimetric in nature employing the fact that the Faraday effect induces polarization changes in the light passing through the sensing element (Faraday element) quantified by the Verdet constant. Although other methods for sensing the magnetic field using Faraday effect have been developed (interferometric to name just a few [4], [5]) this polarimetric method, combined with a solid state sensing element (typically a crystal) is a promising and interesting research stream.

This setup has also been applied for construction of various types of magnetic field sensors and current sensors (via magnetic field sensing) based on Faraday effect and using a Faraday rotator as a sensing element [6]–[8]. All of these require that the Verdet constant be determined in order for the sensor to work properly. The fact that the Verdet constant depends on the temperature and wavelength of the light has been recognized as a potential problem and several methods have been proposed to reduce its influence on the measurement [6], [9], [10]. With monochromatic light sources, change of wavelength can have negative consequences on the sensor since not only Verdet constant depends on the wavelength, but also parameters of other devices present in the measurement chain. To add insult to injury, with semiconductor light source the emitted light spectrum depends on the temperature of the environment, thus causing the temperature to affect the measurement directly and indirectly.

Further, it has been understood that mechanical causes such as vibrations or g shocks can affect the Faraday sensor [11] and steps have been taken to compensate for this. Given the fact that most applications for Faraday sensor are static in nature (power distribution lines) mechanical vibration issues are not of prime concern. However, mounting mechanics for the sensor (mounting for crystal, polarizer, analyzer and so on) are of concern since unwanted intensity modulation of the light can occur if mounts are not designed and manufactured properly.

1.3.   Setups for Measuring Temperature Dependence of the Faraday Effect

Measuring the Verdet constant is a difficult task on its own, let alone when both the wavelength and the crystal temperature are variables. A typical Verdet constant measurement setup (only the constant) would include a reference magnetic induction generator, a stable light source of known wavelength, a setup for polarizing the beam, a setup for conversion of state of polarization to light intensity (usually called the analyzer) and a photodetector. Such a straight setup has been widely used [12], [13], [14], [15] to determine Verdet constant of various materials, some solid, some liquid, to the point that it can even be considered a standard approach. Luckily, such a method also provides a consistent and repeatable way of measuring the Verdet constant, a benefit for collaborative work and result analysis.

A technique for measuring Verdet constant of the terbium gallium garnet (TGG) crystal is presented in [16] that employs a broadband light source with permanent magnet (DC field). The sample is placed in cryo chamber at constant temperature and polarimetric technique is employed to sense the Faraday Effect. A spectrometer determines the intensities at various wavelengths to complete the measurement setup. This setup is somewhat complex, and requires heavy low pass filtering since DC measurement is often easily disturb by EMI and mechanical motion of components. A somewhat different approach is taken in [17] with the same sample in cryostat but with a monochrome laser source and pulsing magnetic field of high intensity. Interestingly, the analyzer is rotated in order to determine the angular position at which the light intensity detected at the photodetector reaches minimum, a sensible proposal from signal processing point of view. Such a method is of course rather slow, since stepping the analyzer requires time, hence the sample must be thermally controlled. An early effort [18] proposes use of commercially available Faraday rotator as a sample (DC

magnetic field) and a chopper-lock in combination used to separate the signal frequency in the frequency domain from the EMI. In order to source various wavelengths, He-Ne, Nd:YAG and Ti:Al_2O_3 have been combined to irradiate the sample.

2. Theoretical overview of optical effects

If an electromagnetic wave, or a photon, hits atoms or molecules of a material, these particles can react in two distinct ways. If the photons were absorbed, an excitation of the particles onto a higher energy level is the result. In this case the band gap of the material is smaller or equal to the energy of the photons ($\hbar\omega$). After the absorption, the excitation of the atom can decay in many different ways. The most important, in the context of optical telecommunications, is the spontaneous emission; in this case the material emits on its part photons with a different energy. This spontaneous emission can in some materials be transmuted into a stimulated emission and is the basis of lasers and the erbium-doped fiber amplifier (EDFA).

2.1. Induced Magneto-Optical Effects

Magneto-Optical Effects (MOE) refer to various changes in the polarization state of light upon interaction with materials possessing a net magnetic moment, including rotation of the Plane of Linearly Polarized (POLP) light (Faraday, Kerr rotation), and the complementary differential absorption of left and right circularly polarized light (LCPL) & (RCPL). In the near visible spectral range these effects result from excitation of electrons in the conduction band. Near X-ray absorption edges, or resonances, magneto-optical effects can be enhanced by transitions from well-defined atomic core levels to transition symmetry selected valence states. Using straight forward symmetry considerations it can be shown that all Magneto Optical (MO) phenomena are caused by the symmetry reduction, in comparison to the paramagnetic state, caused by magnetic ordering. Concerning optical properties this symmetry reduction only has consequences when SO coupling is considered in addition. To calculate MO properties one therefore has to account for magnetism and SO coupling at the same time when dealing with the electronic structure of the material considered[19].

Magneto-optics deals with phenomena arising as a result of interaction between light and matter when the latter is subject to a magnetic field. In the case of magnetically ordered matter (ferromagnetic, paramagnetic, etc.) magneto-optical effects may appear in the absence of an external magnetic field as well. The presence of a magnetic field changes the dispersion curves of the absorption coefficient and leads to the appearance or variation of optical anisotropy. A great number of magneto-optical phenomena are the direct or indirect outcome of the splitting of energy levels in an external or spontaneous magnetic field. This splitting is the Zeeman Effect. Essentially, all magneto-optical effects are consequences of the Zeeman Effect. Optical anisotropy of a magnetized medium manifests itself also in the reflection of light from its surface. Phenomenon arising here are generally referred to as the magneto-optical Kerr effect (MOKE). It refers to the influence of the magnetization of the medium on reflected light.

2.2.   MO Kerr effect

The magneto-optical Kerr effect was discovered by Scottish physicist John Kerr in 1888. He observed that when plane-polarized light is reflected at normal incidence from the polished pole of an electromagnet, it becomes elliptically polarized with the major axis of the ellipse rotated with respect to the plane of polarization of the incident beam

In MO spectroscopy one commonly distinguishes for the incident linearly polarized light between s- and p-polarized light, in which the electric field vector is either normal (s) or parallel (p) to the plane of incident. The MO quantities consequently depend on whether s- or p-polarized incident light.

The Magneto-Optic Kerr Effect (MOKE) is the study of the reflection of polarized light by a material sample subjected to a magnetic field. This reflection can produce several effects, including (A): rotation of the direction of polarization of the light, (B): introduction of ellipticity in the reflected beam and (C): a change in the intensity of the reflected beam. MOKE is particularly important in the

study of ferromagnetic and ferrimagnetic films and materials [20]. There are three "geometries" for MOKE experiments, the Polar, Longitudinal and Transverse geometries. These arise from the direction of the magnetic field with respect to the plane of incidence and the sample surface.
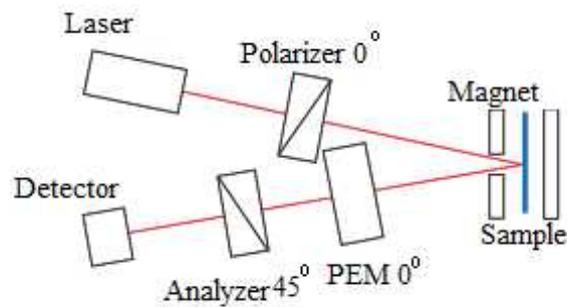
Figure 1 Optical Bench Set-up for Polar MOKE
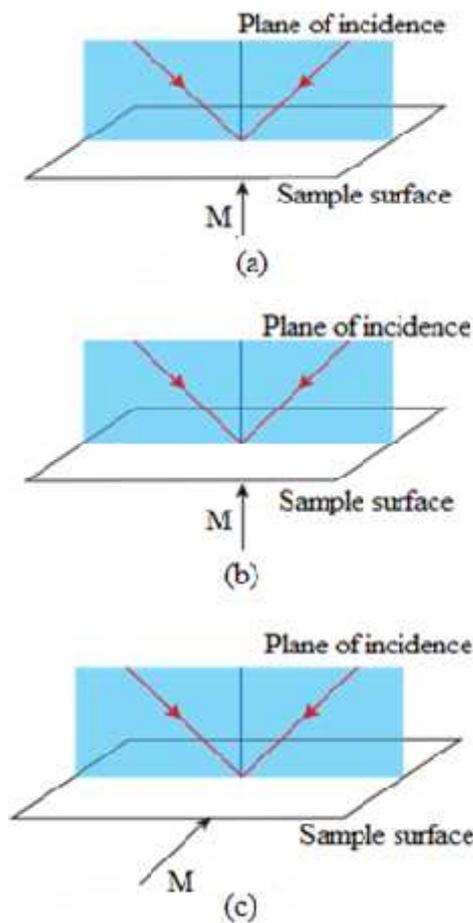
Figure 2 MOKE geometries

a: Polar MOKE geometry, b: Longitudinal MOKE geometry and c: Transverse MOKE geometry

2.3.   MO Faraday effect

If any transparent solid or liquid is placed in a uniform magnetic field, and a beam of plane polarized light is passed through it in the direction parallel to the magnetic lines of force (through holes in the pole shoes of a strong electromagnet), it is found that the transmitted light is still plane polarized, but that the plane of polarization is rotated by an angle proportional to the field intensity. This "optical rotation" is called the Faraday rotation (FR) and differs in an important respect from a similar effect, called optical activity, discovered by M Faraday in 1846.

The angle of rotation is then proportional to the thickness of the material, and the rotary power ρ (rotation angle per unit length) is proportional to the component of the magnetic flux density B in the direction of the wave propagation.

$$\rho = V \tag{2.1}$$

Where *V* is called the Verdet constant [1].

The relationship between the rotation angle of the polarization plane, θ and the magnetic field intensity, B, is given by:

$$\theta = V \, B \, l \tag{2.2}$$

Where l is the path length and V is the proportionality constant, the Verdet constant, specific of the particular crystal.
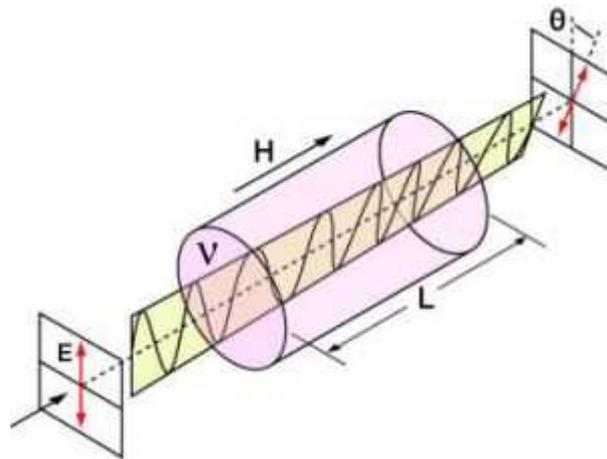
Figure 3 Basic concept of Faraday-rotation

The sense of rotation is governed by the direction of the magnetic field: for B > 0, the rotation is in the direction of a right-handed screw pointing in the direction of the magnetic field. In contrast to optical activity, however, the sense of rotation does not reverse with the reversal of the direction of propagation of the wave. Thus, when a wave travels through a Faraday rotator and then reflects back onto itself, traveling once more through the rotator in the opposite direction, it undergoes twice the rotation [Fig. 4(b)].

(a) Forward wave   (b) Backward wave
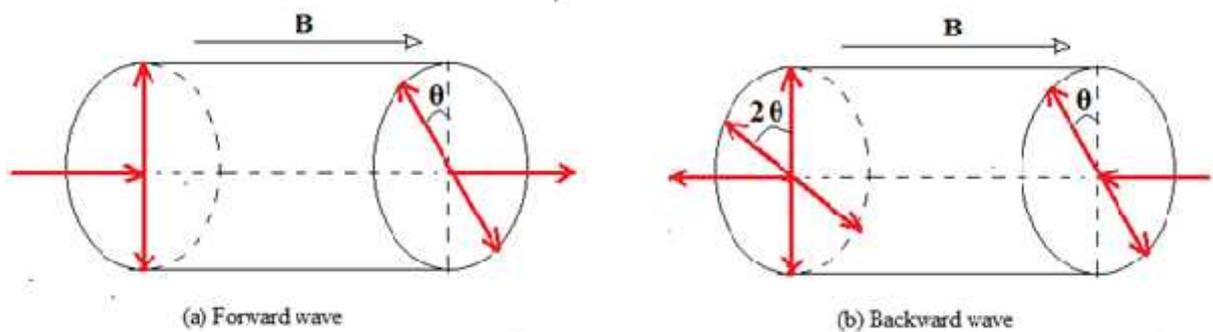
Figure 4 Polarization rotation in a medium exhibiting the Faraday Effect

In (b) it's shown the sense of   rotation in invariant to the direction of travel the wave.

Thin films of these ferromagnetic materials are used to make compact devices[21].

It's sense that in Faraday's effect, the direction of optical rotation, as seen when looking at a beam, is reversed when it passes the light of the opposite material to the direction of the magnetic field. That is, the rotation can be reversed either by changing the direction of the field or the light direction. Light reflection, after passing twice through the medium, has a polarized plane managed by a double angle observed for a single transmission.

Bismuth Germanium Oxide single crystal (Bi12GeO20) is one of Faraday crystals which is under consideration in this theses. It had been shown that a femtosecond pulsed laser irradiation can improve optical properties of $Bi_{12}GeO_{20}$ single crystals, also the effect occurs if the crystals are grown from high purity components was investigated. The samples were irradiated by a femtosecond pulsed laser beam of increasing power. After irradiation, intensity of Raman spectra peaks increased, except for the peak at 203 cm^{-1}, whose intensity decreased. The irradiation also changed the sample color. The induced changes were less intense than was the case when the crystal was grown from components of lesser purity.

Important properties of Bi_{12} GeO_{20} for sensing applications, optical activity, Faraday rotation and absorption were measured and magneto optical quality was calculated and compared[22].

The faraday crystals, is made from material which acts as polarization rotators when placed in a static magnetic field, this property known as Faraday Effect.

The manner of traveling of waves through the Faraday crystal is like that, when a wave travels through a faraday crystal (faraday rotator), reflects back onto itself, and travels once more through the rotator in the opposite direction (undergoes twice the rotation)[21].

Then the Faraday Effect can be exhibiting as

$$D = \varepsilon \ + j\varepsilon_0 \ \gamma \ \times E \qquad\qquad (2.3\ )$$

Where B is the magnetic flux density γ is the constant of crystal called magneto gyration coefficient. The part $\gamma = G$ because in Faraday effect G is independent of K, so the reversal of the direction of propagation does not reverse the sense of rotation of the polarization plane.

Back to the rotation of the polarization plane for $G \ll n_0$ is approximately given by

$$\rho = \frac{-\pi}{\lambda_c n_0} = -\pi \; {}^{B}\!/\!{\lambda_c n_0} \tag{2.4}$$

The Verdet constant given by

$$V = \frac{-\pi}{\lambda_c n_0} \tag{2.5}$$

It is clear that V is function of λ.

2.4.   Theory of Faraday Effect

In this paragraph we will derive Faraday rotation "FR" equation, depending on the elements of the dielectric tensor of a magneto-optical medium such as Bismuth Germanium Oxide single crystal "$Bi_{12}GeO_{20}$" We mainly used theoretical and phenomenological descriptions which also can be found in Ref. [23],[24]. The same theoretical model, which will be presented for the Faraday Effect "FE", can be applied also for the magneto-optical Kerr effect. First let's formulate the problem. Linearly polarized electromagnetic wave propagating through a dielectric material under the influence of external magnetic field changes its state of a polarization after exiting the medium. To solve this kind of a problem one needs to start with Maxwell equations written in a general form:

$$\nabla \times \vec{H} = \frac{1}{c}\frac{\partial \vec{D}}{\partial} + \frac{4\pi}{c}\vec{j} \tag{2.6}$$

$$\nabla \times \vec{E} = -\frac{1}{c}\frac{\partial \vec{B}}{\partial} \tag{2.7}$$

$$\nabla . \vec{B} = 0 \tag{2.8}$$

$$\nabla . \vec{D} = 4\pi \rho_c \tag{2.9}$$

$$\rho = V \tag{2.10}$$

where $\vec{E}$ a $\vec{H}$ are electric and magnetic field intensities respectively, $\vec{D}$ a $\vec{B}$ are electric and magnetic flux densities respectively, ρ_c electric charge density and $\vec{J}$ electric current density and c is speed of light.

If one assumes that material is a linear dielectric then material equations can be presented in following way:

$$\vec{D} = [\epsilon]\vec{E} \tag{2.11}$$

$$\vec{B} = [\mu]\vec{H} \tag{2.12}$$

$$\vec{D} = [\sigma]\vec{E} \tag{2.13}$$

where $[\epsilon]$ is the dielectric tensor, $[\mu]$ is the permeability tensor and $[\sigma]$ is the conductivity tensor. In case under consideration there is a propagation of wave in a ferrimagnetic where conductivity is very small because of insulating properties of ferrimagnets and can thus be ignored. This thesis is only concerned in the FE for optical wavelengths, where $[\mu]$ can be assumed to equal unity. For the ferrimagnets the properties of $[\epsilon]$ can be derived phenomenologically from the considerations of a symmetry. By placing a coordinate system where a ferrimagnet with a cubic symmetry is magnetized along the OZ axis, OX and OY directions for the cubic crystal are equivalent. Then for a transparent ferrimagnet $[\epsilon]$ can be expressed as:

$$[\varepsilon] = \begin{pmatrix} \epsilon & +i\epsilon_1 & 0 \\ -i\epsilon_1 & \epsilon & 0 \\ 0 & 0 & \epsilon_z \end{pmatrix} \tag{2.14}$$

Presence of the external magnetic field or internal spontaneous magnetization of a medium gives rise to a gyrotropy of a medium, so the non-diagonal ϵ_1 components of dielectric tensor are not equal to zero. Finally we also assume that there is no free charge built up so $\rho_0 = 0$.

From the system of Maxwell equations one can solve the wave equation using plane wave approximation and find the values of dielectric tensor elements. Non-diagonal elements related to the refractive indices $n_\pm$ of LCP and RCP lights:

$$n_\pm^2 = \epsilon \pm \epsilon_1 \tag{2.15}$$

In case of transparent approximation as a phase difference between Left circularly -LCP and right circularly polarized RCP lights exists. LP - Linearly polarized light can be represented as a sum of RCP and LCP components as seen shown in Figure 5.

From equation the previous equations it follows that phase velocities of a propagation of a LCP (V_+) and RCP (V_-) components of linearly polarized light wave are different:

$$V_+ = \frac{c}{n_+} \tag{2.16}$$

$$V_- = \frac{c}{n_-} \tag{2.17}$$

which causes a phase difference between RCP and LCP and thus plane of the linearly polarized wave will be rotated by the FR angle:

$$\theta_F = \frac{\omega(n_+ - n_-)z}{c} \tag{2.18}$$

In essence Faraday rotation is cause by the phase difference between the RCP and LCP components of a linearly polarized wave. Fig. 5 shows that linearly

polarized light can be represented as a sum of LCP and RCP lights. So the FR comes from the phase difference of these components of linearly polarized light.

If $\varepsilon \gg \varepsilon_1$ then from equations 2.15 and 2.18 for the FR dependency on dielectric tensor elements will be:

$$\theta_F = -\frac{\omega \varepsilon_1}{c \sqrt{\varepsilon}} \tag{2.19}$$

One can also define specific FR1, which is the FR per medium z thickness, using following equation:

$$\theta_F = -\frac{\omega \varepsilon_1}{c \sqrt{\varepsilon}} \tag{2.20}$$
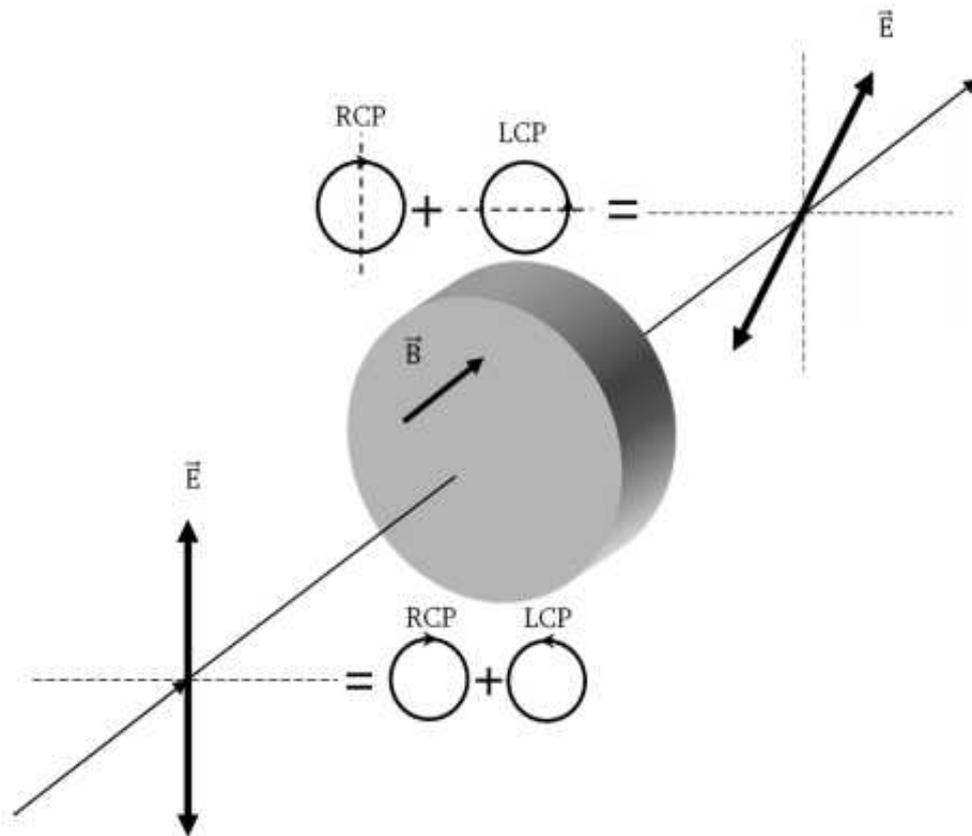
Figure 5 Schematic diagram of Faraday rotation

Formula 2.20 is derived for the following configuration: FR took place for the electromagnetic wave propagating along the direction of the magnetization of a medium. If passing electromagnetic wave gets somehow reflected back into the crystal and again propagated through the material in the opposite direction, the plane of a light will be rotated at the same direction, which means resulting FR will be doubled. For example, if magneto-optical medium is capable of rotating the plane of a linearly polarized light by 45°, then one can use them for the development of optical isolators [18, 25]. The basic operation principle of optical isolators is shown in Figure 6 It is typically used to prevent unwanted feedback into a light source. Non-reciprocal property is also true for microwave frequencies of electromagnetic waves propagating through described magnetized mediums. This allows the creation of radio-frequency devices such as two-port isolators, and three- or four port circulators.
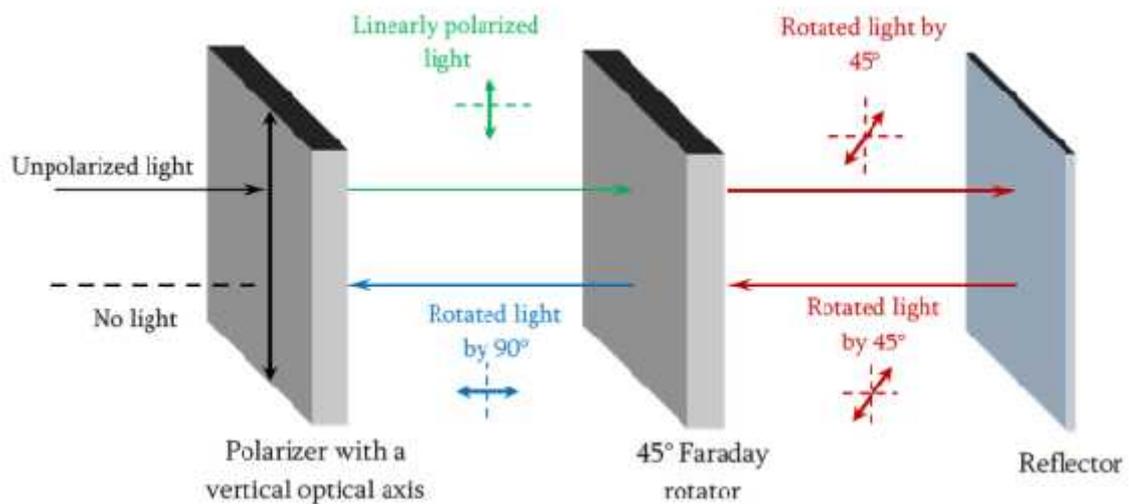
Figure 6 The working principle of optical isolators.
The plane of linearly polarized light is rotated by 90° after two passes through the magnetized 45° Faraday rotator.

In general, components of the dielectric tensor are complex because of the absorption of a medium.

$$\epsilon = \epsilon' + i\epsilon'' \tag{2.21}$$

$$\epsilon' = n^2 - k^2 \tag{2.22}$$

$$\epsilon'' = 2n \tag{2.23}$$

k is the extinction coefficient. The $k_\pm$ extinction coefficients cause different absorptions of the LCP and RCP components. This gives rise to another phenomenon which is magnetic circular dichroism. In result, while exiting from a medium, a light will be also elliptically polarized, which is quantitatively described by the Faraday ellipticity. So for non-transparent ferrimagnetic material FR and Faraday ellipticity will be:

$$\theta_F = \frac{\omega(n_+ - n_-)}{c} = R\left(\frac{\omega\epsilon_1}{c\sqrt{\epsilon}}\right) \tag{2.24}$$

$$\eta_F = \frac{\omega(k_+ - k_-)}{c} = I\left(\frac{\omega\epsilon_1}{c\sqrt{\epsilon}}\right) \tag{2.25}$$

Figure 7 shows schematic diagram of a FR and Faraday ellipticity effects. So the nondiagonal component of the dielectric tensor not only describes the FE, which in other words is magnetic circular birefringence, but also Faraday ellipticity or magnetic circular dichroism. Using equations (2.21 – 2.23) for non-diagonal components we have:

$$\epsilon_1' = \frac{c}{\omega}(n\theta_F - k\eta_F) \tag{2.26}$$

$$\epsilon_1^{"} = \frac{c}{\omega}(k\theta_F + k\ ) \tag{2.27}$$
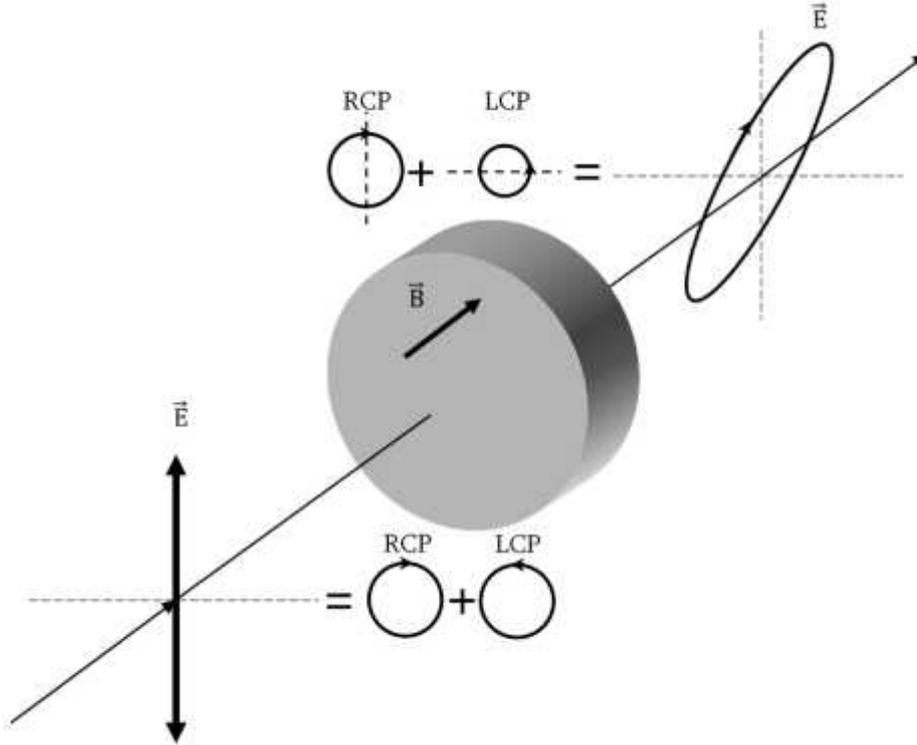
Figure 7 Mechanism of FR and Faraday ellipticity in case of non-transparent medium.

Left circularly -LCP and right circularly polarized RCP lights. LP - Linearly polarized light.

Equations (2.26) and (2.27) show that all the dielectric tensor elements can be calculated if one can experimentally measure θ_F, η_F, n and k. This data of dielectric tensor elements depending on the wavelength can give the possibility to interpret experimental data with microscopic theory of magneto-optical effects.

2.5.   Optical Isolator and Faraday Effect

An optical isolator (OI) is a passive magneto-optic device that only allows light to travel in one direction. Isolators are used to protect a source from back reflections or signals that may occur after the isolator. Back reflections can damage a laser source or cause it to mode hop, amplitude modulate, or frequency shift. In high-power applications, back reflections can cause instabilities and power spikes.

The isolator's function is based on the Faraday Effect. In 1842, Michael Faraday discovered that the plane of polarized light rotates while transmitting through glass (or other materials) that is exposed to a magnetic field. The direction of rotation is dependent on the direction of the magnetic field and not on the direction of light propagation; thus, the rotation is non-reciprocal. The amount of Faraday rotation can be defined from Equation 2.2

The optical isolator consists of an input polarizer, a Faraday rotator with magnet, and an output polarizer. The input polarizer works as a filter to allow only linearly polarized light into the Faraday rotator. The Faraday element rotates the input light's polarization by 45°, after which it exits through another linear polarizer. The output light is now rotated by 45° with respect to the input signal. In the reverse direction, the Faraday rotator continues to rotate the light's polarization in the same direction that it did in the forward direction so that the polarization of the light is now rotated 90° with respect to the input signal. This light's polarization is now perpendicular to the transmission axis of the input polarizer, and as a result, the energy is either reflected or absorbed depending on the type of polarizer.

2.5.1.   Polarization-Dependent Isolators

The Forward Mode

In this example, we will assume that the input polarizer's axis is vertical (0° in Figure 8). Laser light, either polarized or unpolarized, enters the input polarizer and becomes vertically polarized. The Faraday rotator will rotate the plane of polarization (POP) by 45° in the positive direction. Finally, the light exits through the output polarizer which has its axis at 45°. Therefore, the light leaves the isolator with a POP of 45°.

The Reverse Mode

Light traveling backwards through the isolator will first enter the output polarizer, which polarizes the light at 45° with respect to the input polarizer. It then passes through the Faraday rotator rod, and the POP is rotated another 45° in the positive direction. This results in a net rotation of 90° with respect to the input polarizer, and thus, the POP is now perpendicular to the transmission axis of the input polarizer. Hence, the light will either be reflected or absorbed.
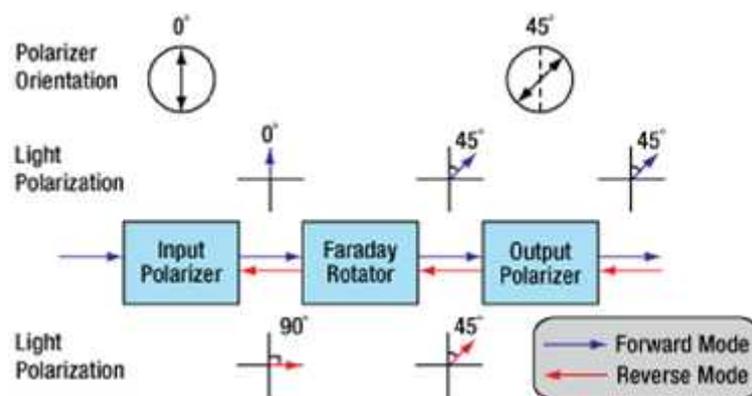
Figure 8 A polarization-dependent isolator. Light propagating in the reverse direction is rejected by the input polarizer.

2.5.2. Polarization-Independent Fiber Isolators

The Forward Mode

In a polarization independent fiber isolator, the incoming light is split into two branches by a birefringent crystal (see Figure 9). A Faraday rotator and a half-wave plate rotate the polarization of each branch before they encounter a second birefringent crystal aligned to recombine the two beams.

The Reverse Mode

Back-reflected light will encounter the second birefringent crystal and be split into two beams with their polarizations aligned with the forward mode light. The faraday rotator is a non-reciprocal rotator, so it will cancel out the rotation introduced by the half wave plate for the reverse mode light. When the light encounters the input birefringent beam displacer, it will be deflected away from the collimating lens and into the walls of the isolator housing, preventing the reverse mode from entering the input fiber.
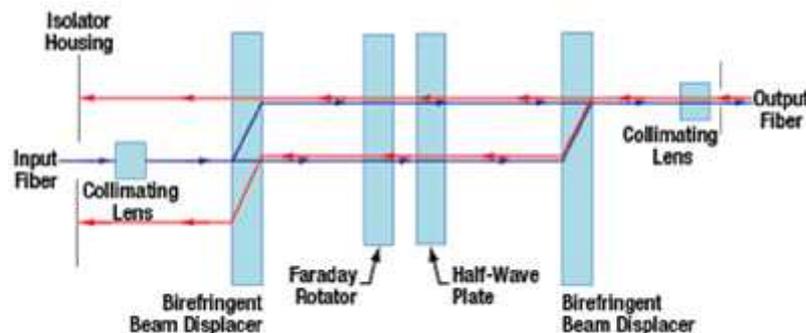
Figure 9. A polarization independent isolator. Light is deflected away from the input path and stopped by the housing.

3.   Crystals

3.1.   Crystal Lattice and Unit Cell

In Crystals the arrangement of atoms in the vacuum arranges to form a geometric pattern. When this pattern is spread to occupy all parts of the material, this means that we have a single crystal if the geometric pattern is stopped when it is called the Grain-Boundaries, the material is then "poly-crystalline," consisting of very small groups of granules or small single crystals in different directions. Unit cell in the science of crystals is the smallest cell, and by conveying it on three vacuum axis consists of crystalline construction. The transfer is parallel to each axis without any rotation of the unit cell. The unit cell is defined by six coordinates: the lengths of the sides (a ,b, and c) and angles between the sides (α β and γ) in Figure 10 .The unit cell contains all elements of symmetry that characterize the crystal. Each corner can occupy one atom, thus making the crystal building body.

A crystal has translational symmetry by definition. If ρ (r) is the electron density within a crystal at r then there exist vectors a, b and c such that: ρ (r) = ρ (r = x · a + y · b + z · c) where x, y and z are integers. Each identical copy (the repeating unit) is called a unit cell. A, b and c are called unit cell vectors. Unit cell vector lengths are a = |a|, b = |b|, c = |c|. α, β and γ describe the angles between unit cell vectors [25].
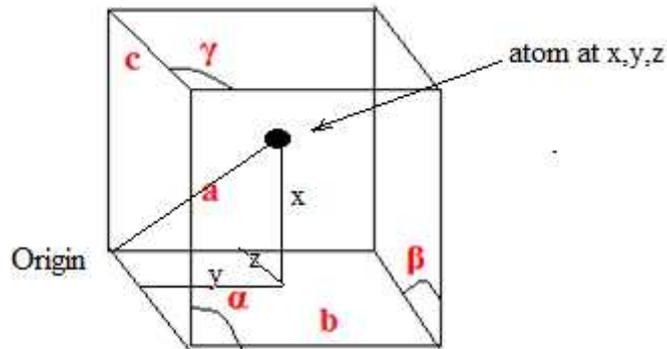
Figure 10 Unit cell example

Cubic body centered (bcc)   Cubic face centered (fcc)   Hexagonal
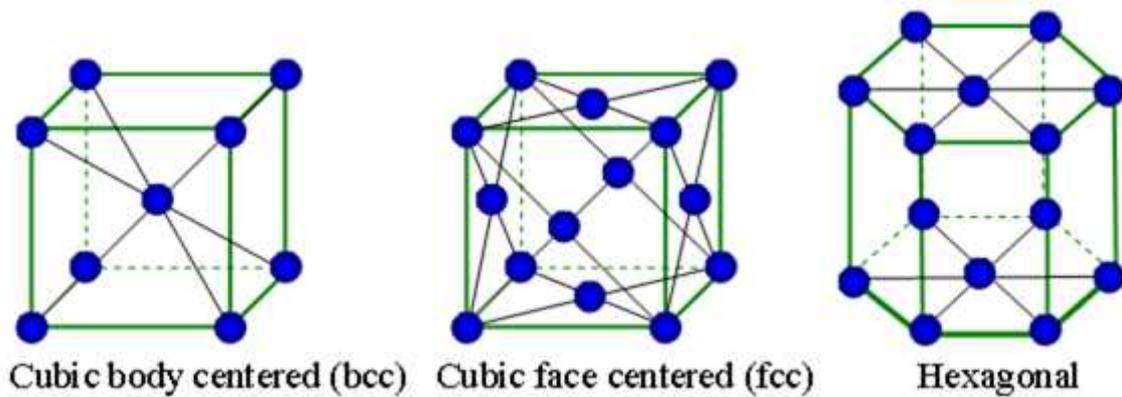
Figure 11 a crystal lattice examples

3.1.1. Fractional coordinates.

Any position within the crystal can be described by r = (u + x)·a + (v + y)·b + (w + z)·c where u, v and w are integers and 0 < x, y, z < 1. • x, y and z are called "fractional coordinates" and describe a position within the unit cell.

3.1.2. Lattice Planes

Lattice planes are planes which pass through the lattice points. Labeled after the fractional position where they first cross the a, b and c axes. If a lattice plane crosses the axes at the fractional coordinates (x, y, z) then the lattice plane is given the Miller indices (h, k, l) equal to (1/x, 1/y, 1/z), as shown in Figure 12
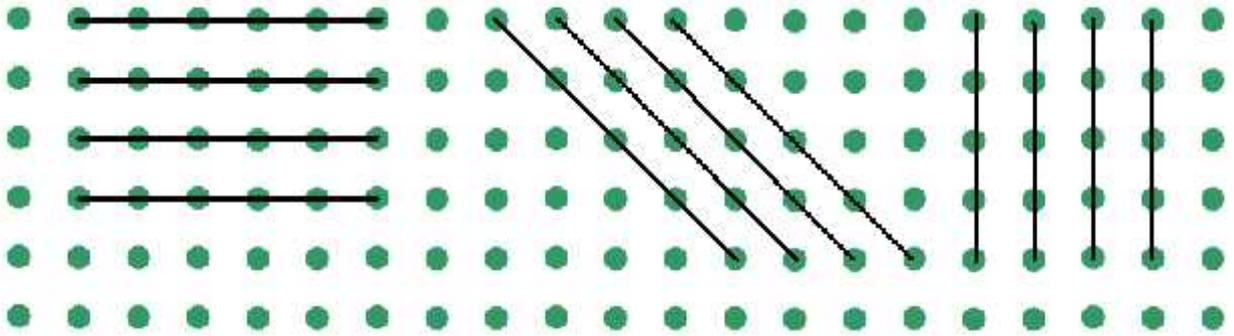
Figure 12 Lattice Planes

3.1.3. Classification of crystals

crystals can be classified based on lattice as: Bravais Lattice crystals and Non-Bravais Lattice crystals, Solid materials are classified according to their magnetic properties to: Diamagnetic materials, Paramagnetic material and Ferromagnetic material. Also crystalline systems can be classified into 7 kinds based on the relations between their lengths of axes a,b,c and angles, α,β,γ (Table 1) [26].

Table 1 Classification of crystals

Crystal type	Axial & angles	Bravais lattice	Lattice shape
Cubic	a=b=c, α=β=γ=90	Simple (P)	
		Body-centered (I)	
		Face-centered (F)	
Tetragonal	a=b≠ c, α=β=γ=90	Simple (P)	
		Body-centered (I)	
Orthorhombic	a≠b≠ c, α=β=γ=90	Simple (P)	
		Body-centered (I)	
		Base-centered (C)	
		Face-centered (F)	
Trigonal	a=b=c, α=β=γ≠90	Simple (R)	
Hexagonal	a=b≠c, α=β=90,γ=120	Simple (P)	
Monoclinic	a≠b≠c, α=γ=90≠β	Simple (P)	
		Base-centered (C)	
Triclinic	a≠b≠c, α≠β≠γ≠90	Simple (P)	

3.2.   Preparation of crystal samples

Single crystals of $Bi_{12}GeO_{20}$ were grown in the air by the Czochralski technique using the MSR 2 crystal puller, Eurotherm temperature controller and the calculated critical crystal diameter, critical rotation rate and pulling rate, as explained in detail in [22]. The system provided small fluctuations in crystal diameter size as well as in melting temperature. The $Bi_{12}GeO_{20}$ seed was oriented in the {111} direction and the charge was a mixture of Bi_2O_3 and GeO_2 in the stoichiometric ratio 6:1. The light yellow crystal samples were obtained using the Bi_2O_3 and GeO_2 purity of 99.999 wt.% and 99.9999 wt.%, respectively. Crystal samples of size 4 mm x 4 mm x 10 mm were cut from the boule and mechanically as well as chemically polished. The technique used to prepare the samples insured maximal sample quality within the limits corresponding to their purity [2].

3.3.   Effects of temperature on the Faraday crystals

Bismuth germanium oxide (BGO) $Bi_{12}GeO_{20}$ is a good choice for the Faraday crystal. It possesses no linear birefringence, can be easily grown by the Czochralski technique, and has a large magneto-optical quality. BGO also possesses optical activity[27] A change of the working temperature of the sensor can reduce sensor sensitivity through temperature dependent optical activity. A change of the working temperature of the sensor can reduce sensor sensitivity through temperature dependent optical activity. On the other hand, the optical activity can provide temperature compensation of the sensor output. A BGO crystal in the Δ/Σ measurement configuration and calcite as the beam splitter was used.

Table 2 BGO crystal properties

Growth parameters	
Melting temperature (K)	1203
Crystal/crucible radius (cm)	1.4/2.2
Crystal rotation rate (rpm)	15
Pulling rate (mmh^{-1})	10
Crystal properties	
Wavelength range, absorption	(1)0.5–6.9μm
coefficients within and value of the	0.4082cm^{-1}
Planck's weight function for the two	0.8672
Semitransparent bands, denoted by (1)	(2) 6.9–9.2μm
and (2)	5.983cm^{-1}
	0.0649
Index of refraction	2.36
Thermal conductivity (W/(mK))	0.18
Radiative–conductive parameter (M)	9.99x10^{-3}
Melt properties	
Density (kg/m^3)	8130
Kinematical viscosity (m^2 /s)	2.09x10^{-6}
Thermal conductivity (W/(mK))	0.345
Specific heat (J/(kgK))	390
Expansion coefficient (1/K)	1.2x10^{-4}

4.   Polarimetric Sensing and Magnetism

4.1.   Introduction

Light is self-propagating electromagnetic oscillations, electric and magnetic fields values vary in a sinusoidal pattern perpendicular to the direction of motion. For example, electric fields could oscillate in the y-direction while magnetic fields oscillate in the z-direction and the wave's motions in the x-direction. Polarization is the state of the e-vector orientation. We may use an xyz coordinate system in which z is the direction of propagation. Since light is a transverse wave, the polarization state can be analyzed by projecting the e-vector onto arbitrary orthogonal axes called x and y, then evaluating these projected components. Viewed across time, the relationship of x and y projections may be fully or partly disordered, and any ordered portion will have a phase and amplitude relation between x and y components. When the electric field vector of all light rays point in the same direction we have "linearly" polarized light. There also exists "circularly" polarized light in which the axis of the electric field rotates, like a spiral staircase. Ordinary light is produced by millions of atoms all vibrating in random directions and is therefore "unpolarized". There are five common ways to convert unpolarized light into (at least partially) polarized light: absorption, reflection, refraction, birefringence, and scattering. Non-polarized light will change to a polarized light after passing through the polarizer (Figure 13)
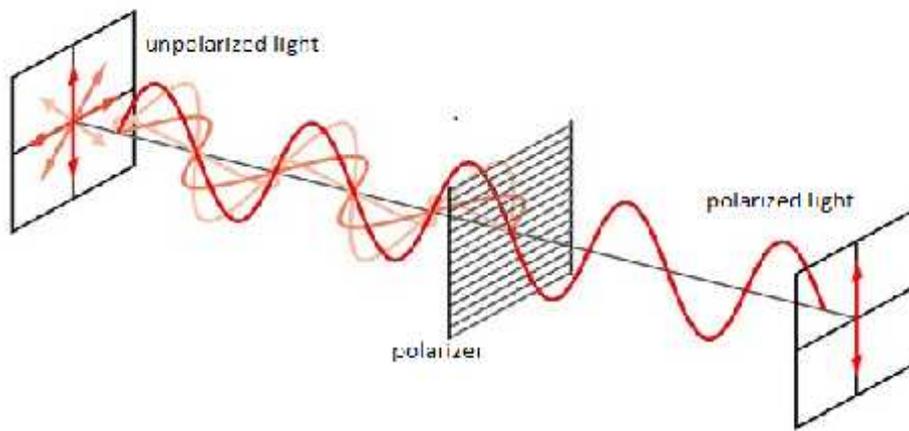
Figure 13 Polarization of light

4.2.   Polarization of Light

Light is electromagnetic wave which contains an electric field and magnetic field fluctuations perpendicular to each other and in the same time those fields perpendicular to the wave propagation direction. According to the definition of polarization, spatial and temporal characteristics of the electric vector of the light wave, determine the light polarization type. If the electric vector of the light is always in one plane, it is called linear polarized light. In this case, the electric vector of light moves on a fixed line and its magnitude and its sign change. The plane, in which the electric vector is fluctuating, is called vibration plane. This plane includes propagation vector K as well as the electric vector. As illustrated in Figure 14 for arbitrary (non-polarized) light wave, the plane, the orientation and the phase of the ellipse generally vary with position.
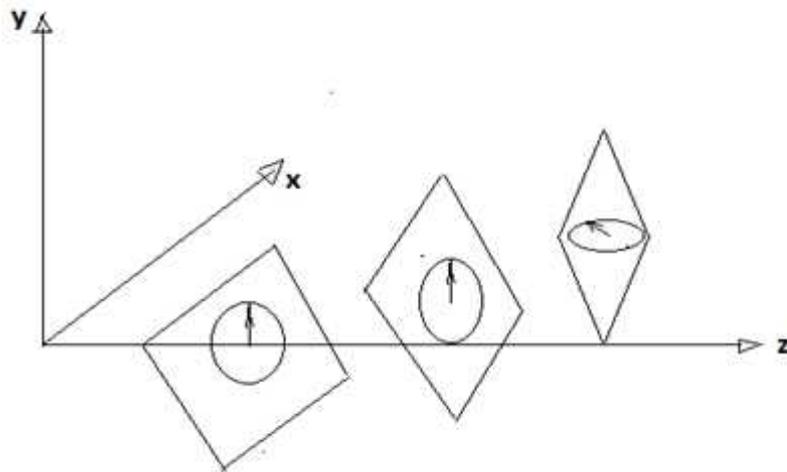
Figure 14 Time course of electric field vector at several positions for arbitrary wave

But in polarized light, the light propagates along direction that lie whiten a narrow cone centered about the optical axis (the z-axis), the electric field vector therefore lies approximately in the transverse plane (the x-y plane), as shown in Figure 15
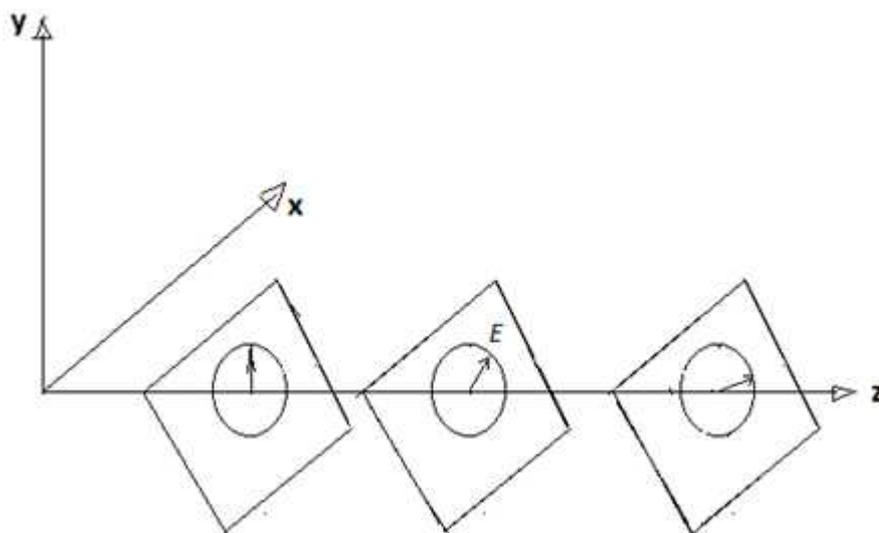
Figure 15 Time course of electric field vector at several positions for polarized wave

So-called optically active materials like, Bismuth Germanium oxide single crystal (Bi12GeO20) have the natural ability to rotate the polarization plane of linearly polarized light.

4.3.   **Theory** of Polarization

If we have two linearly polarized light waves with the same frequency and they are moving in the same direction, and electric vectors of the two waves are in one direction, then the combination of the two waves is a wave with linear polarization. But the electric fields of the waves are perpendicular, the polarization of the resultant wave depends on the relative phase difference between the waves and their amplitude. Consider the two wave components written as:

$$E_x(z,t) = E_{0x}c \quad (\omega \ - k \ ) \tag{4.1}$$

$$E_y(z,t) = E_{0y}c \quad (\omega \ - k \ - \varphi) \tag{4.2}$$

Here E_{0x} and E_{0y} represent the amplitude of the waves and k is the propagation constant that is equal to $2\pi / \lambda$, and λ is the wavelength of light. φ is the relative phase difference between the waves and $\omega = 2\pi$, where f is the frequency of light. The equation indicates waves that are moving in the direction of z axis. In this case, the resultant wave is equal to:

$$E(z,t) = iE_x(z,t) + jE_y(z,t) \tag{28}$$

Where, i and j are the unit vectors on the x and y axis. The resultant wave according to the last equation can have linear or circular or elliptical polarization. The amplitude of polarized wave can be calculated from:

$$E = \sqrt{E_{0x}^2 + E_{0y}^2}$$ (4.4)

If in the Eq.3.2, φ is zero or an integer multiple of 2π, two waves are in phase. Thus, the resultant wave is a wave with **linear polarization**.

If Eq. 3.1 and Eq.3.2 has the following:

$$\varphi = \frac{-\pi}{2} + 2m$$ (3.5)

$$E_{0x} = E_{0y} = E_0$$ (4.6)

Then the resultant wave is equal to:

$$E_{z.t} = E_0\big(i\iota \quad (\omega \ - k_z)\big) + s_i \quad (\omega \ - k_z)$$ (4.7)

Here the amplitude of E is constant but its direction changes with time and movement is not limited to one plane. Such a wave is called clockwise circular polarized wave. In this case the electric vector end moves on a circle, and the wave is said to be circularly polarized

Circularly polarized light is a special case of elliptically polarized light in which the two components have a 90° phase difference and the electric field vector describes a circular cross section spiral. When viewed looking towards the source, a right circularly polarized beam has a light vector that describes a clockwise circle, while left circularly polarized light describes an anti-clockwise circle.

4.3.1.   The Polarization Ellipse

Expressing A_x and A_y in terms of their magnitudes and phases

$$A_x = a_x e \quad (j\emptyset_x)\&$$
$$A_y = a_y e \quad (j\emptyset_y)$$

(4.8)

The electric field vector can be written as

$$E(z,t) = E_x \hat{x} + E_y \hat{y}$$

(4.9)

and its x-y components is E_x & E_y Where

$$E_x = a_x c \left[2\pi \left(t - \frac{z}{c} \right) + \phi_x \right]$$
$$E_y = a_y c \left[2\pi \left(t - \frac{z}{c} \right) + \phi_y \right]$$

(4.10)

and they are periodic functions of $t - \frac{z}{c}$ oscillating at frequency v.

The electric field vector components seems as a parametric equations of ellipse

$$\frac{E_x^2}{a_x^2} + \frac{E_y^2}{a_x^2} - 2\cos\emptyset \frac{E_x E_y}{a_x a_y} = s \quad {}^2\emptyset$$

(4.11)

Where $\emptyset = \emptyset_y - \emptyset_x$ is the phase difference.

At a fixed value of z, the tip of the electric vector rotates periodically in the x-y plane tracing out the ellipse.

At a fixed t, the locus of the tip of the electric field vector follows a helical trajectory in the space lying on the surface of elliptical cylinder. The electric field rotates as the wave advances repeating its motion periodically for each distance corresponding to a wavelength $\lambda = \frac{c}{v}$.

The state of polarization of the wave is determined by the shape of the ellipse, which is depends on two parameters - the ratio of magnitudes a_y/a_x and the phase difference $\emptyset = \emptyset_y - \emptyset_x$ The size of the ellipse on the other hand, determines the intensity of the wave $I = \left(a_x^2 + a_y^2\right)/2\eta$ where η is the impedance of the medium, or from other hand in this case the said to be elliptically polarized. The electric field of elliptically polarized light consists of two perpendicular linear components with any amplitude and any phase difference. The resulting electric field describes an ellipse.

.
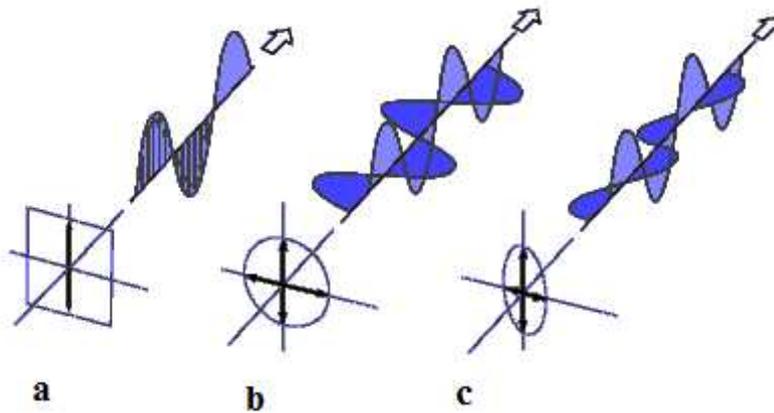
Figure 16 polarization of electromagnetic waves

a: Linear polarization, b:Circular polarization and c Elliptical polarization

The summation of two orthogonally polarized plane waves (Figure 17) that are out of phase results in elliptically polarized light[28]
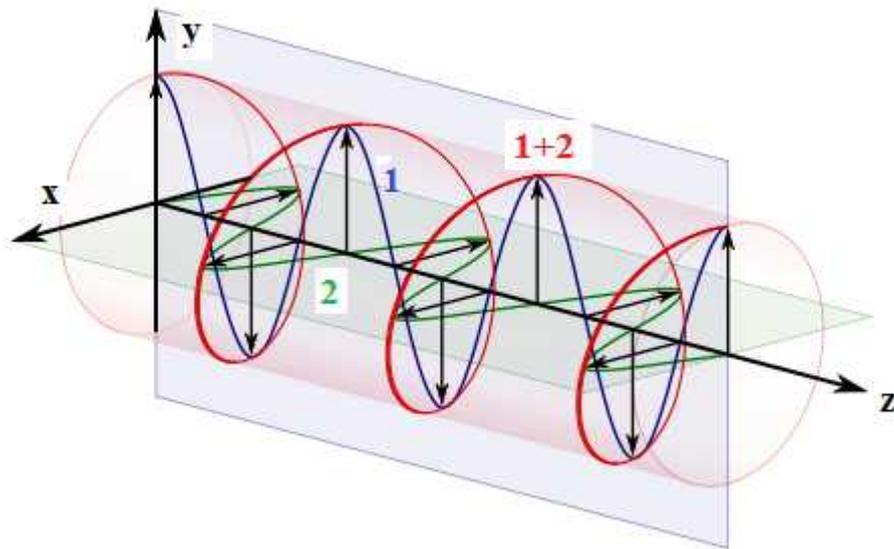
Figure 17 Combination of two orthogonally polarized plane waves

If we imagine that we see a circularly polarized light field throughout space at an instant in time as in Figure 17 the electric field vector spirals as we move along the z - direction. If the sense of the spiral with time matches that of a common wood screw oriented along the z -axis, the polarization is called right handed. If instead the field spirals in the opposite sense, then the polarization is called left handed. The field shown in Figure 18 is an example of left-handed circularly polarized light. An equivalent way to view the handedness convention is to imagine the light impinging on a screen as a function of time. The field of a right-handed circularly polarized wave rotates counter clockwise at the screen, when looking along the k direction (towards the front side of the screen). The field rotates clockwise for a left-handed circularly polarized wave.
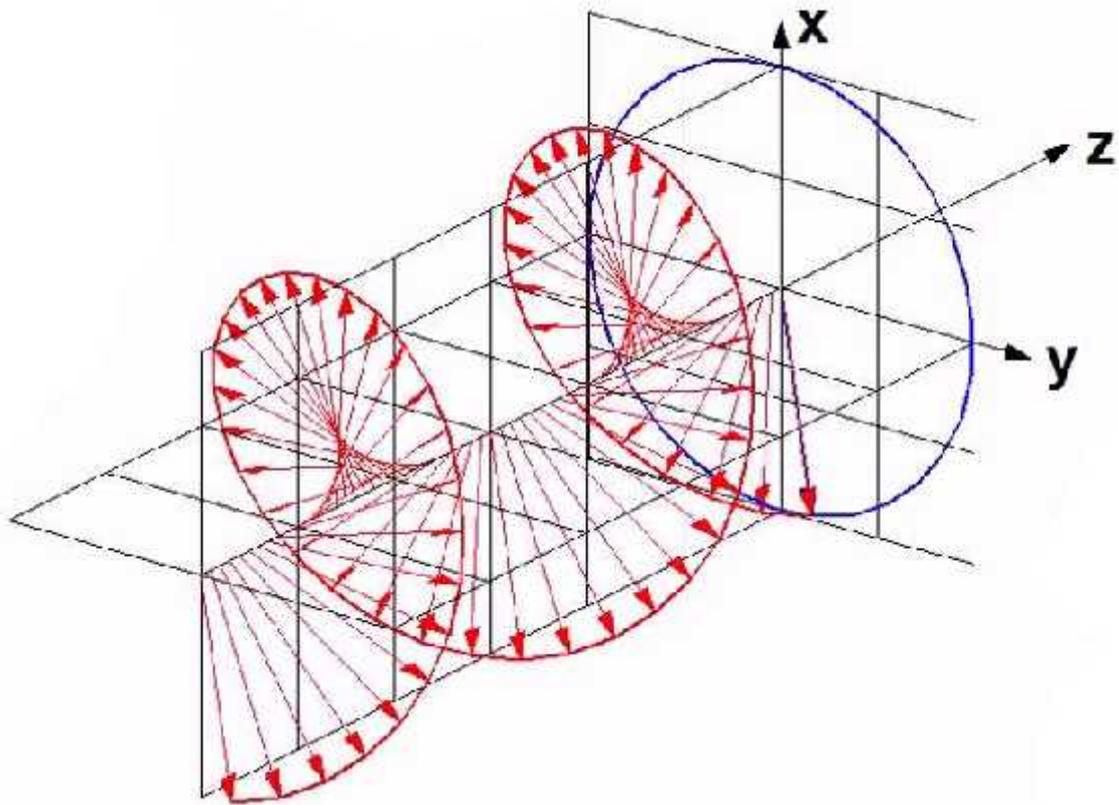
Figure 18 Circularly (Right hand) Polarization

4.3.2. Polarizers

In order to select a specific polarization of light, we need to use polarizer. Dependent on the application you can select the right polarizer. Polarizers can be describe by several types, reflective, dichroic, and birefringent. **Reflective polarizers** transmit the desired polarization and reflecting others. An example of this is Wire grid polarizers. Its consisting of many thin wires arranged parallel to each other, and the light that is polarized along these wires will reflected, while light that is polarized perpendicular to these wires will transmitted. Other reflective polarizers use Brewster's angle. Brewster's angle is a specific angle of incidence under which only s-polarized light is reflected. The reflected beam is s-polarized and the transmitted beam becomes partially p-polarized. **Dichroic**

polarizers absorb a specific polarization of light, transmitting the rest; modern nano-particle polarizers are dichroic polarizers. **Birefringent polarizers** rely on the dependence of the refractive index on the polarization of light. Different polarizations will refract at different angles and this can be used to select certain polarizations of light. Unpolarized light can be considered a rapidly varying random combination of p- and s-polarized light. An ideal linear polarizer will only transmit one of the two linear polarizations, reducing the initial unpolarized intensity I_0 by half,

$$I = \frac{I_0}{2} \tag{4.12}$$

For linearly polarized light with intensity I_0, the intensity transmitted through an ideal polarizer, I, can be described by Malus' law,

$$I = I_0 c \cdot {}^2\theta \tag{4.13}$$

Where θ the angle between the incident linear polarization and the polarization axis. We see that for parallel axes, 100% transmission is achieved, while for 90° axes, also known as crossed polarizers, there is 0% transmission. In real world applications the transmission never reaches exactly 0%, therefore, polarizers are characterized by an extinction ratio, which can be used to determine the actual transmission through two crossed polarizers.

4.3.3.   Birefringent Polarizers

Birefringence is the optical property of a material having a refractive index that depends on the polarization and propagation direction of light. These optically anisotropic materials are said to be birefringent (or birefractive). The birefringence is often quantified as the maximum difference between refractive indices exhibited by the material. Crystals with non-cubic crystal structure are often birefringent, as are plastic under mechanical stress.

Birefringence is responsible for the phenomenon of double refraction whereby a ray of light, when incident upon a birefringent material, is split by polarization into two rays taking slightly different paths [9]. Birefringence can be quantified by measuring the changes in polarization of light waves. This method of measurement is called polarimetry. A special method, called dual polarization interferometry, is used to measure birefringence of lipid bilayers. Birefringence can be classified as intrinsic or stress-induced birefringence.

Intrinsic Birefringence – This type of birefringence is caused by the anisotropy present in the crystals. The atomic arrangement of the crystal itself is the source of birefringence. Examples are calcite, tourmaline, etc.

Stress-Induced Birefringence, This type of birefringence is caused due to the stresses imposed on the material. Materials such as glass or plastics show strain birefringence

Linear Birefringence

Linearly birefringent uniaxial crystalline materials are characterized by having a unique axis of symmetry, called the optic axis, which imposes constraints upon the propagation of light beams within the crystal. Two modes are permitted, either as an ordinary beam polarized in a plane normal to the optic axis, or as an extraordinary beam polarized in a plane containing the optic axis. Each of the beams has an associated refractive index, such that both the electric field (wave normal) velocities and the beam (ray) angles of refraction are different. It is this latter property that enables suitably cut and oriented prisms of birefringent materials to act as polarizers and polarizing beam splitters.

Circular Birefringence

If a plane polarized beam propagates down the optic axis of a material exhibiting circular birefringence it is resolved into two collinear circularly polarized beams, each propagating with a slightly different velocity. When these two components emerge from the material, they recombine into a plane polarized beam whose plane of polarization is rotated from that of the incident beam. This

effect of producing a progressive rotation of the plane of polarization with path length is called optical activity, and is used to produce optical rotators.

4.3.4. Calcite (CaCO₃)

Calcite is a widely preferred choice of material, owing to its very high birefringence, wide spectral transmission and the availability of reasonably sized crystals. Unfortunately, calcite cannot be manufactured synthetically. Only natural crystals exist which limits the maximum size with good optical quality. It has the advantage of being non-hygroscopic, so that protection from the atmosphere is not necessary, though it is a fairly soft crystal and is easily scratched. We have perfected a number of proprietary processes for cutting, grinding and polishing perfect optical surfaces on calcite prisms, routinely achieving flatnesses down to lambda/8 over several cm with 10/5 scratch dig. These skills are evident in the high quality of the finished components, and enable our polarizers to be used with very high peak power lasers.

The Calcite crystal was used in this thesis experiments because it has good birefringence.

An unpolarized ray incident on a face of a calcite crystal will in general be refracted into two rays, propagating in different directions within the crystal, and with orthogonal plane polarizations. This separation is used in various forms of birefringent polarizer. In the Nicol prism, made of calcite (Figure 19) the two rays are separated at a layer of transparent cement within the calcite, arranged so that one of these rays is removed by total internal reflection. The single emergent ray is accurately linearly polarized.
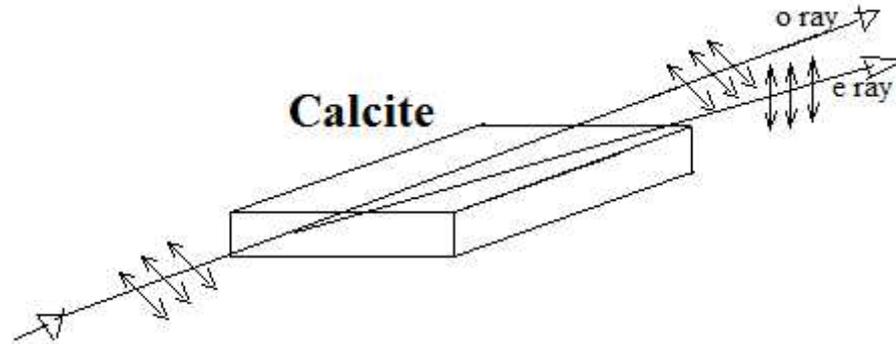
Figure 19 Nicol prism, made of calcite

The advantage over the Nicol prism, made of calcite is symmetry: both components are transmitted through similar paths in the crystal, and any absorption is the same for both.

4.4.   Optical Activity

Optical rotation (OR) or optical activity (OA) is the rotation of linearly polarized light as it travels through certain materials which will acts as natural polarization rotators. Their normal modes are waves that are circularly, rather than linearly polarized; waves with right- and left-circular polarizations travel at different phase velocities. We demonstrate below that an optically active medium with Right Hand Circularly Polarization (RHCP) and Left Hand Circularly polarization (LHCP) phase velocities C_0/n_+ and C_0/n_- acts as a polarization rotator with an angle of rotation

$$\pi(n_- - n_+)\,{}^d\!/_{\lambda_0} \tag{4.14}$$

that is proportional to the thickness of the medium d[21]. The rotatory power (rotation angle per unit length) of the optically active medium is therefore

$$\rho = \frac{\pi}{\lambda_0}(n_- - n_+) \tag{4.15}$$

Where λ_0 is the wavelength of the light in vacuum, n_- & n_+ the reflective indices RHCP and LHCP respectively.

Although the optical activity of crystals could provide us with valuable information about the bonding, nature of constituent atoms in crystals. When light strikes a parallel-sided plate of an optically active crystal, it splits into two elliptically polarized waves, and they propagate in the crystal having the same ellipticity but opposite sense of rotation. Their major axes, which are at right angles to one another, coincide with the principal vibration directions (optical principal axes) that would exist for this light if the crystal were not optically active. [26]

4.5.   Orthogonal polarization technique with two beams

The two orthogonally polarized light beams needs for sensing the Faraday rotation and measuring rotation angle θ.

To achieve the two polarized light beams Calcite crystal was used instead of polarizing prism. After the light (laser beam) passing through the beam displacer (birefringent crystal) will spatially divide the laser beam into components ordinary and extraordinary rays.

Irradiations of both beams depend on the source intensity in the someway.

By using the difference-over-sum method $\frac{\Delta}{\epsilon}$ [4] we can calculate angle $\square$ which tell us how the polarization plane angle change due to Faraday crystal.

Back to beam displacer and its splitting of light passing through it, before we turn on the current (absence of magnetic field) electric field amplitude of two light waves emerging from beam displacer are $E_1 \& E_2$ we define angle $\emptyset_c a \ \tan(\emptyset_c) = {E_1}/{E_2}$
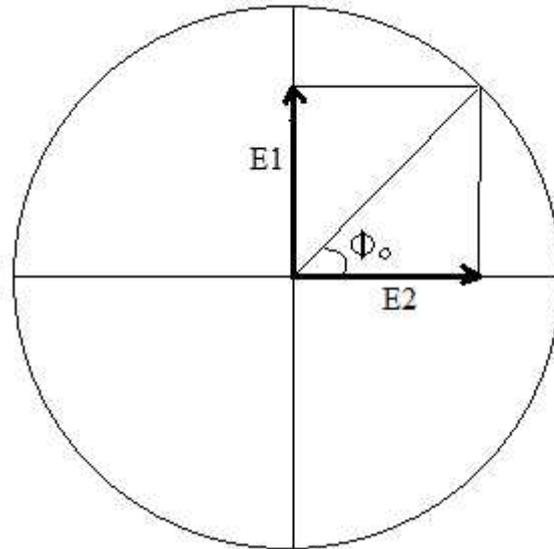
Figure 20 absence of magnetic field B=0

At the moment we turned on the current (presence of magnetic field$B \neq 0$) the polarization plane of light incident on birefringent crystal is rotated in the counter clockwise direction by angle∅.
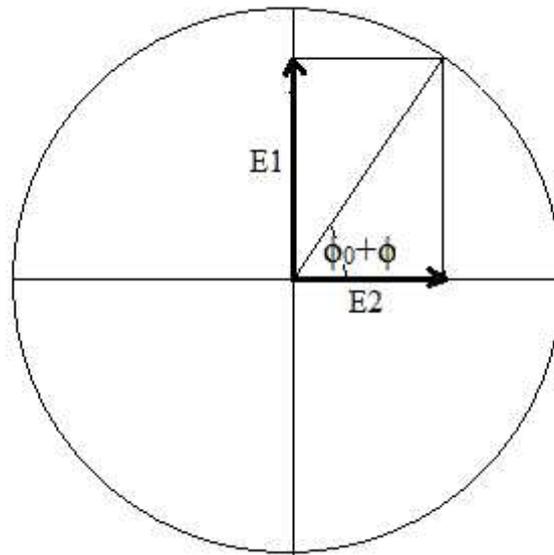
Figure 21presence of magnetic field B≠0

The birefringent crystal converts the rotation of the polarization plane into intensity modulation of two light beams.

If E_0 is the electric field amplitude of the laser beam light wave, then we can write:

$$U_1 = k_1 E_0^2 s\text{i}^2 \emptyset_0)$$
$$U_2 = k_2 E_0^2 c\text{i}^2 \emptyset_0)$$
$$U_1 = k_1 E_0^2 s\text{i}^2 (\emptyset_0 + \emptyset)$$
$$U_2 = k_2 E_0^2 c^2 (\emptyset_0 + \emptyset)$$

(4.16)

Where k_1 and k_2 are constant that include all optical losses as well as optoelectronic conversion efficiency, and U_1 and U_2 are voltages after transimpedance stage.

Then:

$$t\text{i}(\emptyset_0) = \sqrt{\frac{U_1}{U_2}\frac{k_2}{k_1}}$$

(4.17)

In order to detect gains of two beams identically we need to set $k_1 = k_2$ without any crystals, by adjusting the parameters of the transimpedance stages. In order to set the quiescent point of the sensor to the desired value $\emptyset_0 = {}^{\pi}/_4$ the calibration of the two gains is necessary. At this point we introduced crystals. To see the changes of the angle due to faraday crystal we need to see the changes of plane polarizations which is a function of U_1&U_2 ($U_1=U_2$ at $\emptyset_0 = {}^{\pi}/_4$). In the absence of the magnetic field, $U_1 = U_2$. The angle $\emptyset_0 = {}^{\pi}/_4$ provides maximum system sensitivity. Output signals U_1 , U_2 are then:

$$U_1 = \frac{k_1 E_0^2}{2}(1 + \sin 2\theta) \& U_2 = \frac{k_2 E_0^2}{2}(1 - \sin 2\theta)$$

(4.18)

And the desired result $\emptyset$ is:

$$\emptyset(B) = \frac{1}{2}\arcsin\left[\frac{U_1 - U_2}{U_1 + U_2}\right]$$

(4.19)

At any time $U_1 \neq U_2$ we have some value of rotation of plane polarization defined by angle($\emptyset$), this result is result is valid only if $k1(t) = k2(t)$ at any moment of time.

In our case, $k1 = k2$ is equivalent to

$$\frac{d_2}{d} = -\frac{d_1}{d} \; o \; \left|\frac{d_2}{d}\right| = \left|\frac{d_1}{d}\right| \tag{4.20}$$

We can also calculate magnetic induction B and electric current I that induced B.

From the last equation it can be noticed that the angle of rotation of plane polarization (θ) does not depend on the light source intensity and optical losses of light beam incident on the birefringent crystal.
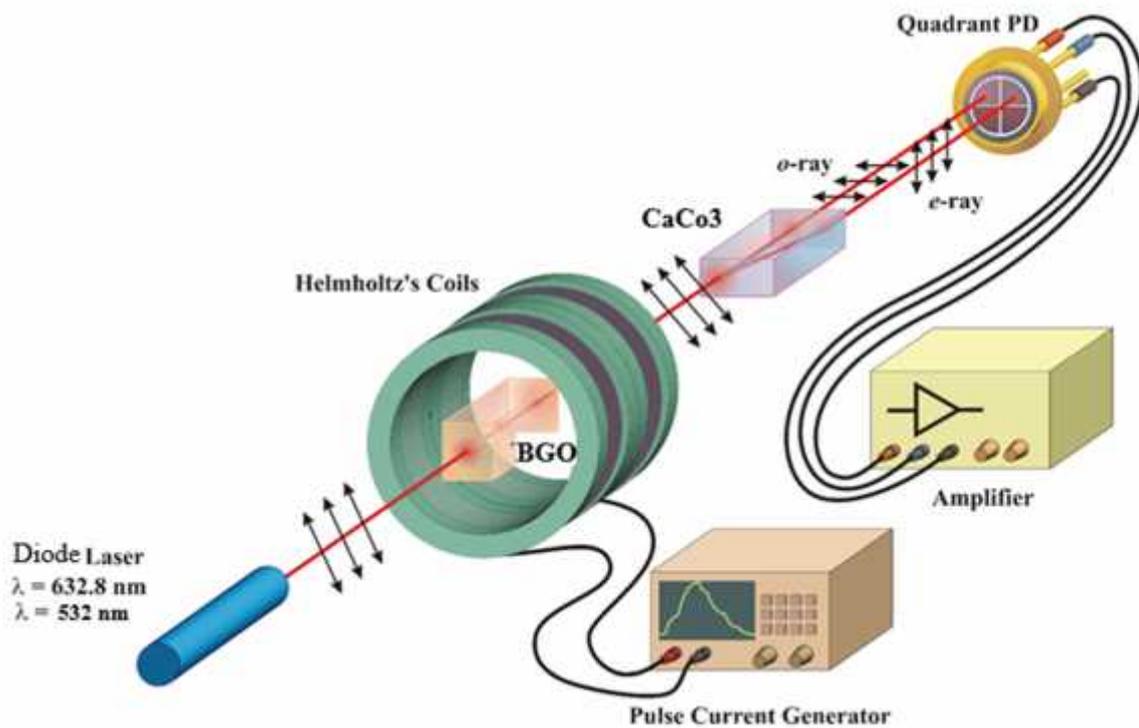
Figure 22 Twin- beam current sensing concept

4.6. The Helmholtz coils

A Helmholtz coil is a device for producing a region of nearly uniform magnetic field, named after the German physicist Hermann von Helmholtz. It consists of two solenoid electromagnets on the same axis. Besides creating magnetic fields, Helmholtz coils are also used in scientific apparatus to cancel external magnetic fields, such as the Earth's magnetic field. The magnetic field in a point on the axis of circular coil with a single winding of radius R is given by

$$B(z) = \frac{\mu_0 . I}{2} . \frac{R^2}{(z^2 + R^2)^{3/2}} \tag{4.21}$$

Where z is the distance from the center to the axial field point, μ_0 is the permeability of free space ($4\pi.10^{-7}$ Tm/A), I is the current passing through the coils (A), R is the radius of the coil (m), s is a distance between the coils (m). For two coils placed a distance apart, both carrying the same current I, with z=0 at the midpoint of the coils, we have

$$B_1(z) = \frac{\mu_0 . I}{2} . \frac{R^2}{\left(\left(z + \frac{s}{2}\right)^2 + R^2\right)^{3/2}} \tag{4.22}$$

$$B_2(z) = \frac{\mu_0 . I}{2} . \frac{R^2}{\left(\left(z - \frac{s}{2}\right)^2 + R^2\right)^{3/2}} \tag{4.23}$$

The total magnetic field from the two coils can be obtained using the principle of superposition [2]

$$B(z) = \frac{\mu_0 . I. R^2}{2} \left(\left(\left(z + \frac{s}{2}\right)^2 + R^2\right)^{-3/2} + \left(\left(z - \frac{s}{2}\right)^2 + R^2\right)^{-3/2}\right) \tag{4.24}$$

46

If we derivative the last equation with respect to z to express the homogeneity of the magnetic field, the resulting yields that $\frac{d}{d} = 0$ at z =0 which is true for all values of s[29].
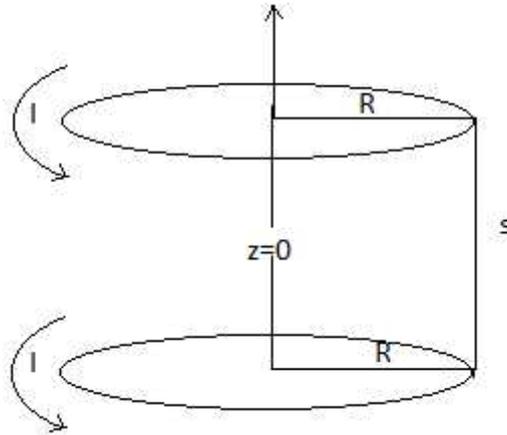
Figure 23 Dimensions of the coils

Now if we differentiate of B(z) with respect to z, we get the result with not automatically zero for z=0 (corresponding to the midpoint of the two coils).

But we have only one exception at s=R, in this case we get the most homogeneous magnetic field if we place the tow coils in a distance equal to their radius with such configuration the coils are called "Helmholtz coils"[29]. That's why this kind of coils has been selected as a source of magnetic field in the experiments.

The equation of magnetic field due to Helmholtz coils can be now written as

$$B(z) = \frac{\mu_0 . I . R^2}{2}\left(\left(\left(z + \frac{R}{2}\right)^2 + R^2\right)^{-3/2} + \left(\left(z - \frac{R}{2}\right)^2 + R^2\right)^{-3/2}\right)$$

(4.25)

4.6.1.   Calculating the magnetic field of Helmholtz coils

In the previous section, we saw out how to produce a homogeneous magnetic field theoretically. In Table 3 one can see the result of normalized magnetic field of Helmholtz at a fraction distance Z/R, the current (I amp) was sent through the wire. For our magnetic sensor the variable homogeneous magnetic field of 0.73 - 1.32 mT was produced, we realize that this is actually a significant magnetic field. Hence we have to optimize the design of the Helmholtz coils and "bring the best out of everything we got". The upper limit as to how much current we can send through the wire, together with the very strong field, results in a large number of windings on the Helmholtz coils.

Table 3 Normalized magnetic field of Helmholtz at a fraction distance Z/R, where Z: distance from midpoint between, R: radius of each coil.

Z[m]	B[T]	Z/R	B/Bmax	Z[m]	B[T]	Z/R	B/Bmax
-0.115	0.000732225	-1	0.619264	0.005	0.001182406	0.043478	0.999996
-0.11	0.000771806	-0.9565	0.652739	0.01	0.001182334	0.086957	0.999935
-0.105	0.000811633	-0.91304	0.686422	0.015	0.001182024	0.130435	0.999673
-0.1	0.000851303	-0.86957	0.719972	0.02	0.001181206	0.173913	0.998981
-0.095	0.000890367	-0.82609	0.75301	0.025	0.001179524	0.217391	0.997558
-0.09	0.000928351	-0.78261	0.785134	0.03	0.001176562	0.26087	0.995054
-0.085	0.000964768	-0.73913	0.815933	0.035	0.001171872	0.304348	0.991087
-0.08	0.000999141	-0.69565	0.845003	0.04	0.001165003	0.347826	0.985278
-0.075	0.001031029	-0.65217	0.871972	0.045	0.001155535	0.391304	0.97727
-0.07	0.001060049	-0.6087	0.896515	0.05	0.001143107	0.434783	0.96676
-0.065	0.001085904	-0.56522	0.918381	0.055	0.00112745	0.478261	0.953517
-0.06	0.001108396	-0.52174	0.937404	0.06	0.001108396	0.521739	0.937404
-0.055	0.00112745	-0.47826	0.953517	0.065	0.001085904	0.565217	0.918381
-0.05	0.001143107	-0.43478	0.96676	0.07	0.001060049	0.608696	0.896515
-0.045	0.001155535	-0.3913	0.97727	0.075	0.001031029	0.652174	0.871972
-0.04	0.001165003	-0.34783	0.985278	0.08	0.000999141	0.695652	0.845003
-0.035	0.001171872	-0.30435	0.991087	0.085	0.000964768	0.73913	0.815933
-0.03	0.001176562	-0.26087	0.995054	0.09	0.000928351	0.782609	0.785134
-0.025	0.001179524	-0.21739	0.997558	0.095	0.000890367	0.826087	0.75301
-0.02	0.001181206	-0.17391	0.998981	0.1	0.000851303	0.869565	0.719972
-0.015	0.001182024	-0.13043	0.999673	0.105	0.000811633	0.913043	0.686422
-0.01	0.001182334	-0.08696	0.999935	0.11	0.000771806	0.956522	0.652739
-0.005	0.001182406	-0.04348	0.999996	0.115	0.000732225	1	0.619264
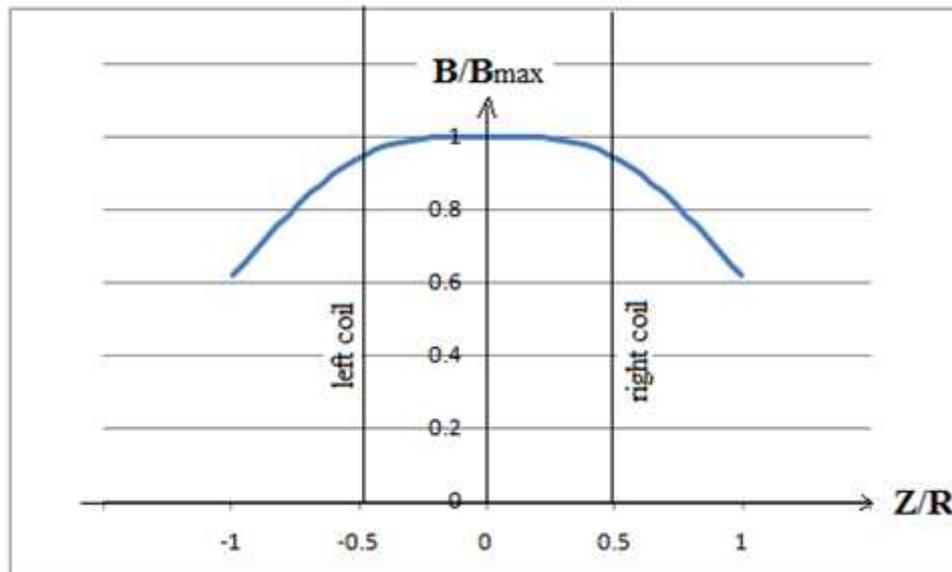
Figure 24 The magnetic field of the Helmholtz coils vs of the distance.

4.6.2. Specification of Helmholtz coils used in experimental work

Type: Dual coils: Helmholtz

Number of turns per coil: N=240

Total resistance: 1.8Ω

Maximum current: I_{max} = 6A (in our experiment we apply the current to the coils 4.14A)

Diameter of wire: d = 2.10^{-3}m

Radius of the coils (distance from the center to the beginning of the first winding): R=$11.5.10^{-2}$ m

Distance between coils = R

Number of wire in one row of the coil: =17

Width of each coil: a=17x d = 34.10^{-3} m

4.6.3. Experimental verification of the magnetic induction created by the Helmholtz Coils

Since almost all equations tend to treat the magnetic induction in the crystal to be of uniform nature it would be advisable that the magnetic induction intensity be verified by an experiment. Such verification involves a magnetic sensor (preferably of different nature than the Faraday sensor) that can sample the magnetic induction value in a small volume, much smaller than the size of the Helmholtz coils. Since the coil volume is quite large, positioning the sensor and sampling the volume must be automated to avoid positioning mistakes. Further, an automated data acquisition system must be constructed to acquire the induction value and present the data in an understandable manner.

Scanning configuration is presented in Figure 25. A DC memsic magnetic sensor (SH) was mounted on a plastic arm (L profile) that can move in a volume of interest using two motorized positioner (MP) mounted in a cross configuration. Using this arrangement it was possible to scan bigger part of the coils volume in one plane (a 2D scan). This motorized stage block can be controlled from the PC to automatize movements and readings. Sensor data was acquired using measurement acquisition system (MAS) also connected to PC to deliver data. Coils (HC) were powered from the current source (CS).

.
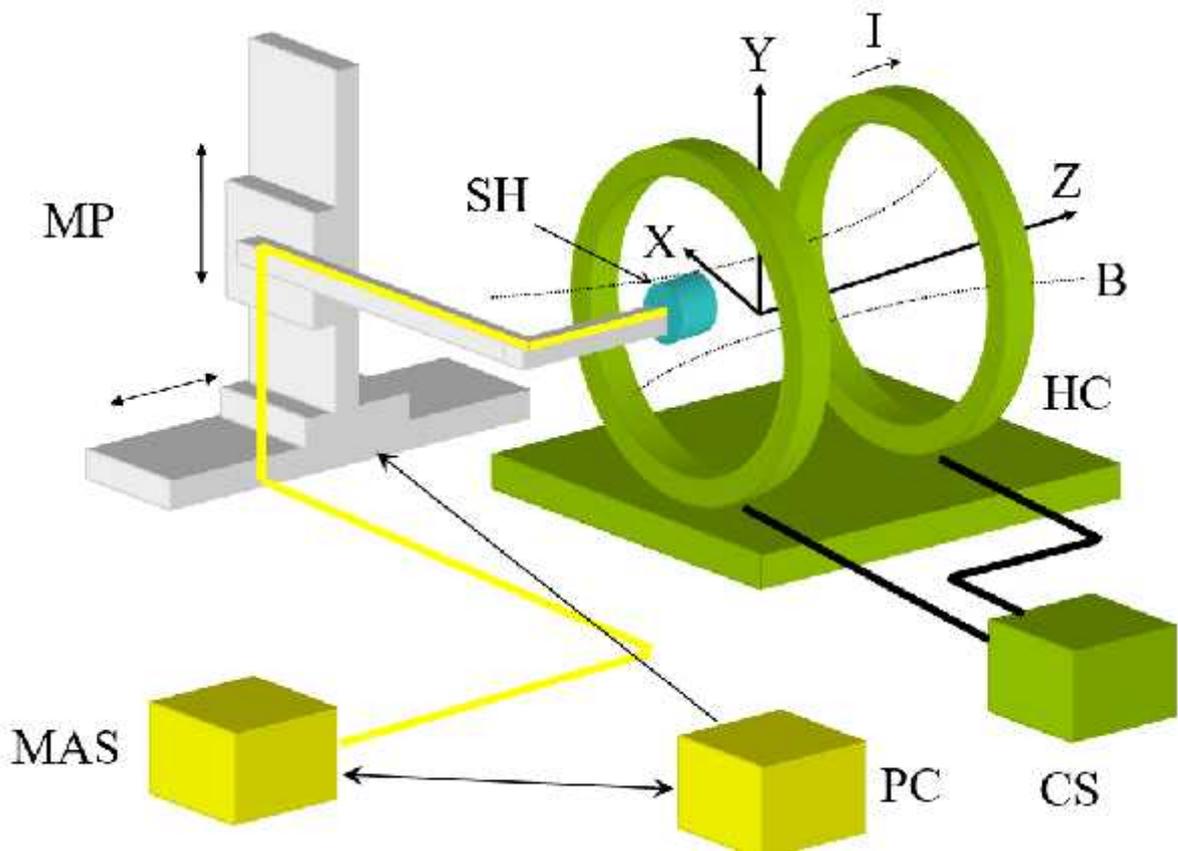
Figure 25 Setup for magnetic induction measurement.

A typical scan run involves PC controlling the motor stages thus moving the sensor across a plane inside (typically y-z) and outside of the coils (x-y). A constant current is powering the coils in order to make induction stable and readings of the induction value were recorded for induction component in the desired plane. We have chosen to measure induction in the Z direction since crystals are oriented in the same way. It was possible to move the sensor in a 200 mm x 200 mm area that is much bigger than the crystal and covers the area in the coils.

A sample scan in y-z plane is presented in Figure 26 with the crystal shape symbolically placed in the magnetic induction in position that will be used for Faraday Effect measurement. It can be seen that the induction is not constant in the entire coil volume, yet it is very constant (surface plot is flat) in the area covered by the crystal.
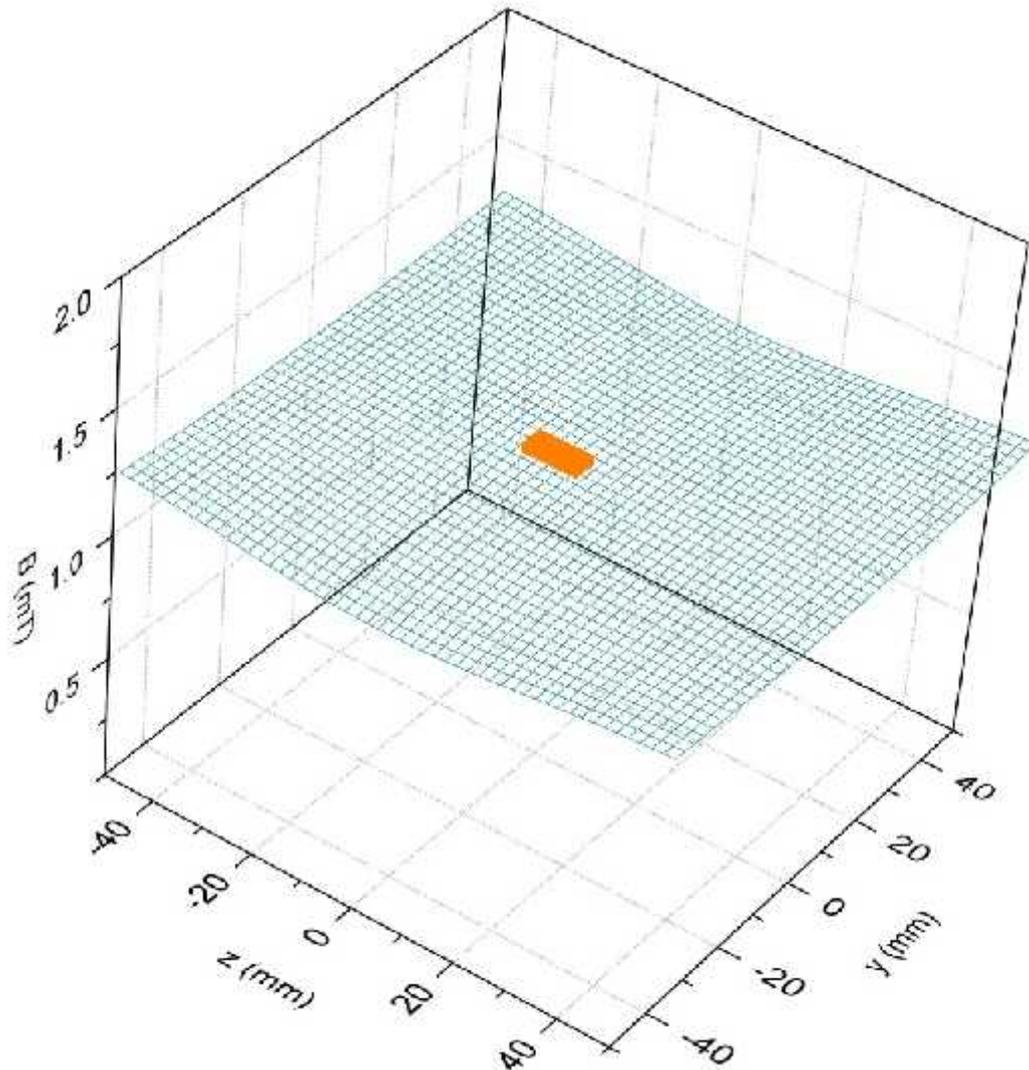
Figure 26 Magnetic induction inside the Helmholtz coils with symbolic shape of the crystal immersed in the homogeneous magnetic field.

This data matches the induction flatness calculated in Figure 24 and proves that it is correct to assume that the induction value is constant in the crystal volume. In addition, magnetic field outside the coils is seen in Figure 27 for information purposes.
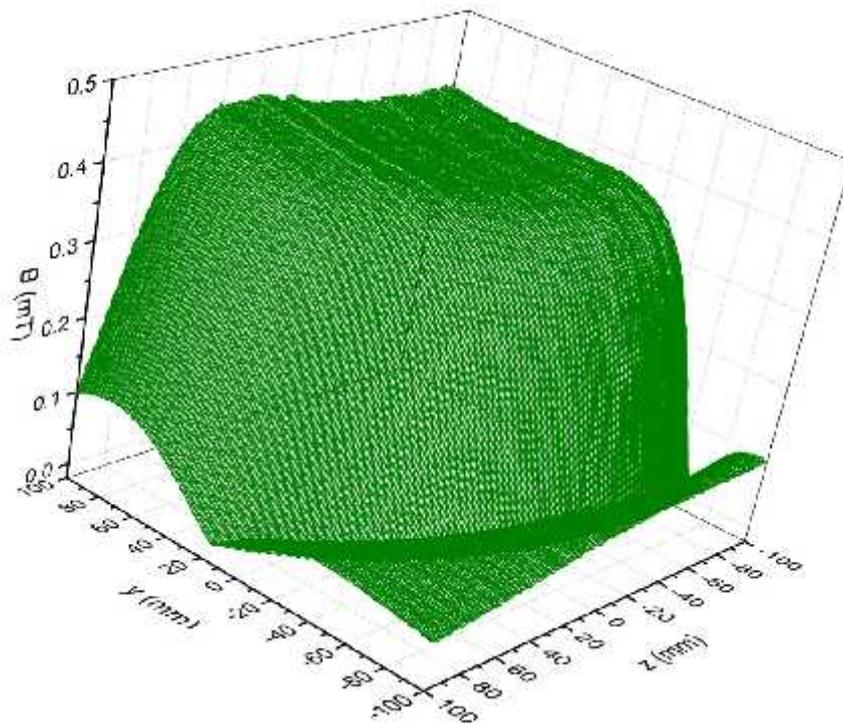
Figure 27 Magnetic induction Outside Coils

5.   Polarimetric Faraday Effect Magnetic Field Sensor

5.1.   Sensor configurations

In order to detect the Faraday e ect there are two most common sensor configurations transmition and reflection configurations. In this chapter these two configurations will be described as well as the components.

5.1.1.   Transmissive configuration

Transmissive configuration used to measure optical activity, no magnetic field applied during measurement
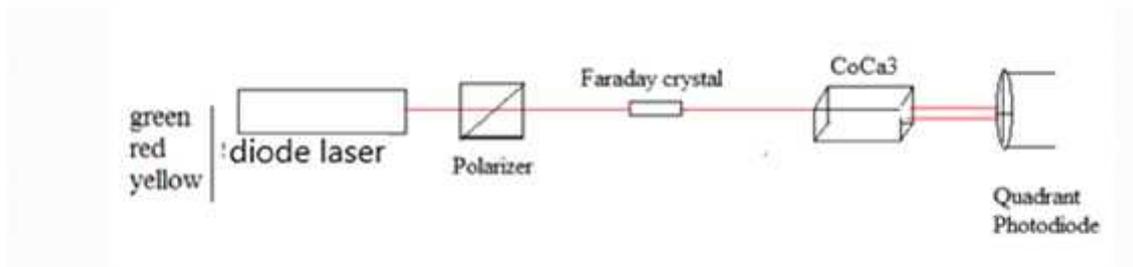
Figure 28 Transmition configuration

5.1.2.   Reflective configuration

Reflective configuration used to measure Verdet constant since optical activity cancels out in back propagation. The Verdet constant of a magneto-optical material such as $Bi_{12} GeO_{20}$ Crystal shows up in the calculation of the rotation of polarized light in a medium submerged in a magnetic field. The amount of rotation is given by $\theta = 2VBd$, where θ is the angle of rotation of linear polarized light, V is the Verdet constant , B is the magnetic field (assumed to be constant over the length of the crystal), and d is the path length over which the magnetic field interacts with the light.
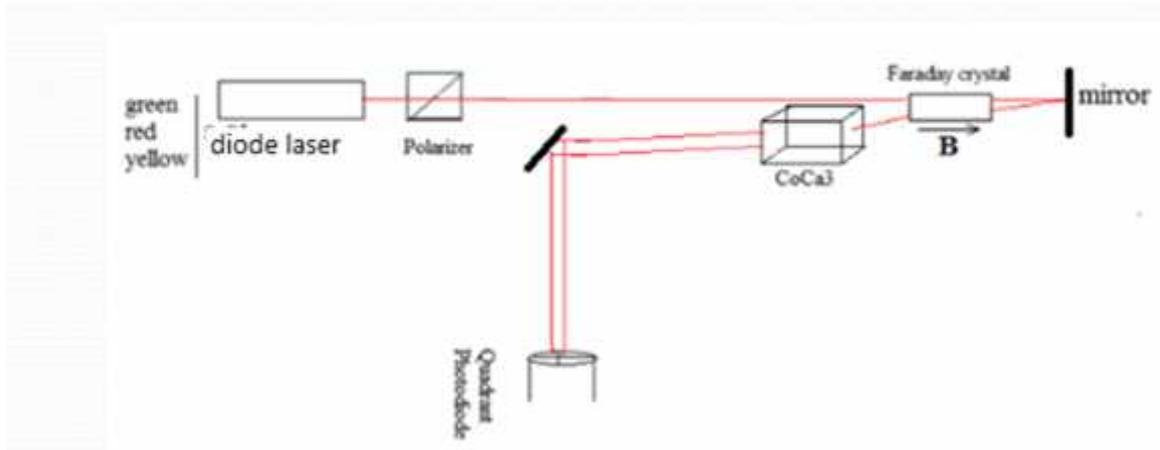
Figure 29 Reflective configuration

5.2.   Sensors Classification

∫   Intrinsic

Sensors use fiber as the sensing element

∫   Extrinsic

The magnetic field is measured using a crystal

For Faraday rotation detection, polarimetric configuration was used instead of interferometric, because it has some advantages.

∫   Small amount of optical material that is needed

∫   Short and simple optical path

∫   The capability of constructing a portable sensor

Less signal processing

5.3.   Extrinsic Faraday Effect Sensor

The measuring head depicted in Figure 30 was designed to provide two antiphase channels for θ measurement and normalization. The two channels designed for the Faraday rotation detection are constructed in reflection so that the optical activity as a reciprocal effect cancels. In addition, the optical path is doubled as well as the Faraday rotation. Since the refraction index of BGO crystal is 2.55 there is sufficient light in the reflection without any kind of mirror.

Transmition axis of polarizers in front of receiving fibers are mutually perpendicular and at 45° with respect to the transmition axis of the polarizer in front of the source fiber to obtain maximum sensitivity[30]. Thus voltages after paired transimpedance stages are:

$$U_1 = \frac{k_1 I_0}{2}\left(1 + \sin(2\theta)\right)$$
$$U_2 = \frac{k_2 I_0}{2}\left(1 + \sin(2\theta)\right) \tag{5.1}$$

where I_0 is the intensity of the light source, and k is a constant that includes all optical losses, as well as the optoelectronic conversion efficiency. Angle θ is determined by the difference over the sum method and is therefore independent on the light source fluctuations (normalization):

$$\theta = 2V = \frac{1}{2}\sin^{-1}\left(\frac{U_1 - U_2}{U_1 + |U_2|}\right) \tag{5.2}$$

10 mm long BGO crystal with 6 mm radius was used
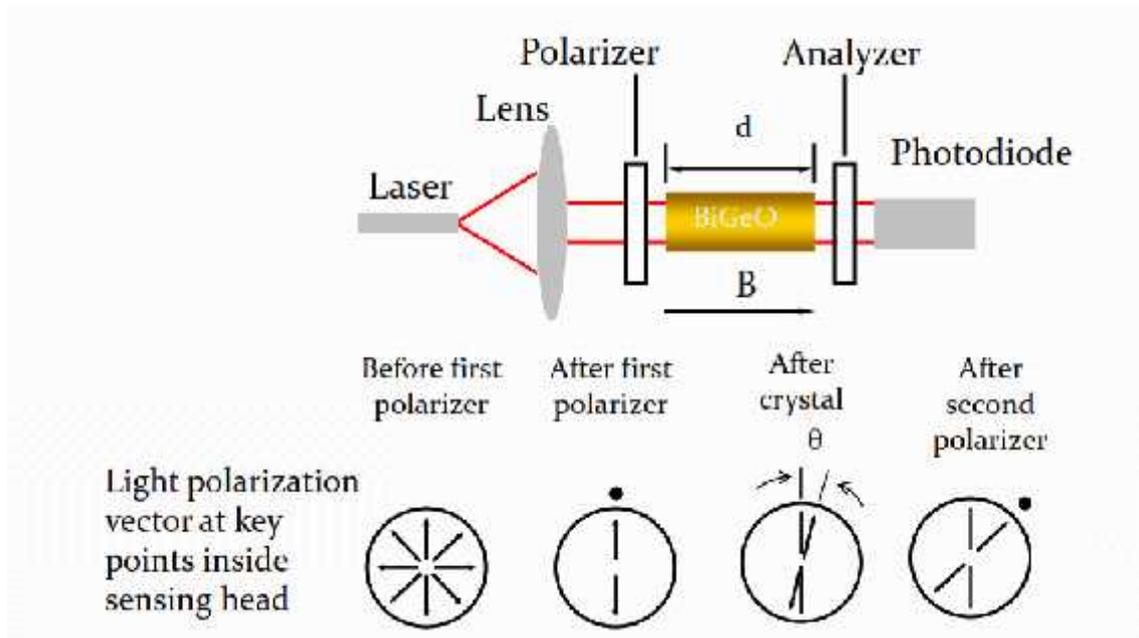
Figure 30 Extrinsic Faraday Effect Sensor construction

Fiber-optic current sensor (FOCS) technique. It's also based on the Faraday Effect. There is several advantages of FOCS compared to conventional iron-core current transformers: the immunity to electromagnetic interference noncontact measurement, high dynamic range, compact design, and impossibility of explosion and high bandwidth that allows harmonic analysis of current represent the main advantages of FOCS from the electrical power industry aspect.

6.   Non-contact temperature measurement of the Faraday crystal temperature

Temperature is one expression for the kinetic energy of the vibrating atoms and molecules of matter. This energy can be measured by various secondary phenomena, e.g., change of volume or pressure, electrical resistance, electromagnetic force, electron surface charge, or emission of electromagnetic radiation. The most frequently used temperature scales are Celsius and Fahrenheit, which divide the difference between the freezing and boiling points of water into 100° and 180°, respectively. The thermodynamic scale begins at absolute zero, or 0 Kelvin, the point at which all atoms cease vibrating and no kinetic energy is dissipated. K = –273.15°C = –459.67°F

6.1.   Non-contact temperature measurement advantages

The noncontact temperature measurement has some advantages which is absent in contact temperature measurement methods.

It is fast (in the ms range) time is saved, allowing for more measurements and accumulation of data (determination of temperature field).

It facilitates measurement of moving targets (conveyor processes).

Measurements can be taken of hazardous or physically inaccessible objects (high-voltage parts, great measurement distance).

Measurements of high temperatures (greater than 1300°C) present no problems. In similar cases, contact thermometers cannot be used, or have a limited life.

There is no interference, no energy is lost from the target. For example, in the case of a poor heat conductor such as plastic or wood, measurements are extremely accurate with no distortion of measured values, as compared to measurements with contact thermometers.

There is no risk of contamination and no mechanical effect on the surface of the object; thus wear-free. Lacquered surfaces, for example, are not scratched and soft surfaces can also be measured.

6.1.1. Determining Emissivity

There are various methods for determining the emissivity of an object. First, you can find the emissivity of many frequently used materials in a table. Emissivity tables also help you find the right wavelength range for a given material, and, so, the right measuring device. Particularly in the case of metals, the values in such tables should only be used for orientation purposes since the condition of the surface (e.g. polished, oxidized or scaled) can influence emissivity more than the various materials themselves. It is possible to determine the emissivity of a particular material yourself using different methods. To do so, you need a pyrometer with emissivity setting capability.

Heat up a sample of the material to a known temperature that you can determine very accurately using a contact thermometer (e.g. thermocouple). Then measure the target temperature with the IR thermometer. Change the emissivity until the temperature corresponds to that of the contact thermometer. Now keep this emissivity for all future measurements of targets on this material.

At a relatively low temperature (up to 260°C), attach a special plastic sticker with known emissivity to the target. Use the infrared measuring device to determine the temperature of the sticker and the corresponding emissivity. Then measure the surface temperature of the target without the sticker and re-set the emissivity until the correct temperature value is shown. Now, use the emissivity determined by this method for all measurements on targets of this material.

Create a blackbody using a sample body from the material to be measured. Bore a hole into the object. The depth of the borehole should be at least five times its diameter. The diameter must correspond to the size of the spot to be measured with your measuring device. If the emissivity of the inner walls is greater than 0.5, the emissivity of the cavity body is now around 1, and the temperature

measured in the hole is the correct temperature of the target. If you now direct the IR thermometer to the surface of the target, change the emissivity until the temperature display corresponds with the value given previously from the blackbody. The emissivity found by this method can be used for all measurements on the same material.

If the target can be coated, coat it with a matte black paint ("3-M Black" from the Minnesota Mining Company or "Senotherm" from Weilburger Lackfabrik , either which have an emissivity of around 0.95). Measure the temperature of this blackbody and set the emissivity as described previously [31].

Notice that, the second thickness were used in our case for measuring the samples emissivity.

6.2.   Infrared Measurement Technology, Pyrometry

The recognition of radiation heating of a hot body belongs to the basic experiences of mankind. The measurement of temperature radiation (infrared radiation) to determine the temperature of a body is one of the newer temperature measurement methods in the industrial sector.

In a pyrometer the thermal radiation emanating from a body is focused by a lens on a radiation receiver. As receiver, thermocouples, photomultipliers, photoresistors, photo-diodes etc. can be used. The "heat radiation "generates an electrical signal which can be utilized to determine the temperature.

A differentiation is made between the various pyrometer types, such as total radiation pyrometer, spectral pyrometer, radiation density pyrometer, distribution pyrometer and disappearing filament pyrometer.

Pyrometers can replace contacting thermometers only in a few applications. More often they are used to supplement contacting methods in areas where no or unsatisfactory results occur. Basically, pyrometry, in contrast to contacting methods, can only measure the heat on the surface.

The application focus is the temperature measurement on surfaces, on fast moving parts, on objects with minimal heat capacity or heat conductivity, on objects with fast changing temperatures and on objects which are not easily accessible. Also products which cannot be touched due to sterilization or processing constraints (e.g. in the food industry) are suitable for temperature measurements with pyrometers [32].

6.3.   Thermal Imaging Cameras

In principle the thermal imaging camera has the same physical effects as a pyrometer.

However, the pyrometers determine the average temperature of the entire surface being measured while the thermal imaging camera produces a thermal picture of the object. Area sensors are used for this. The number of available detector elements defines the quality of the picture.

Thermal imaging cameras are primarily used today to monitor and control machinery, electrical and mechanical systems and objects in which localized heating could damage or destroy the item as well as where heat losses are to be determined.
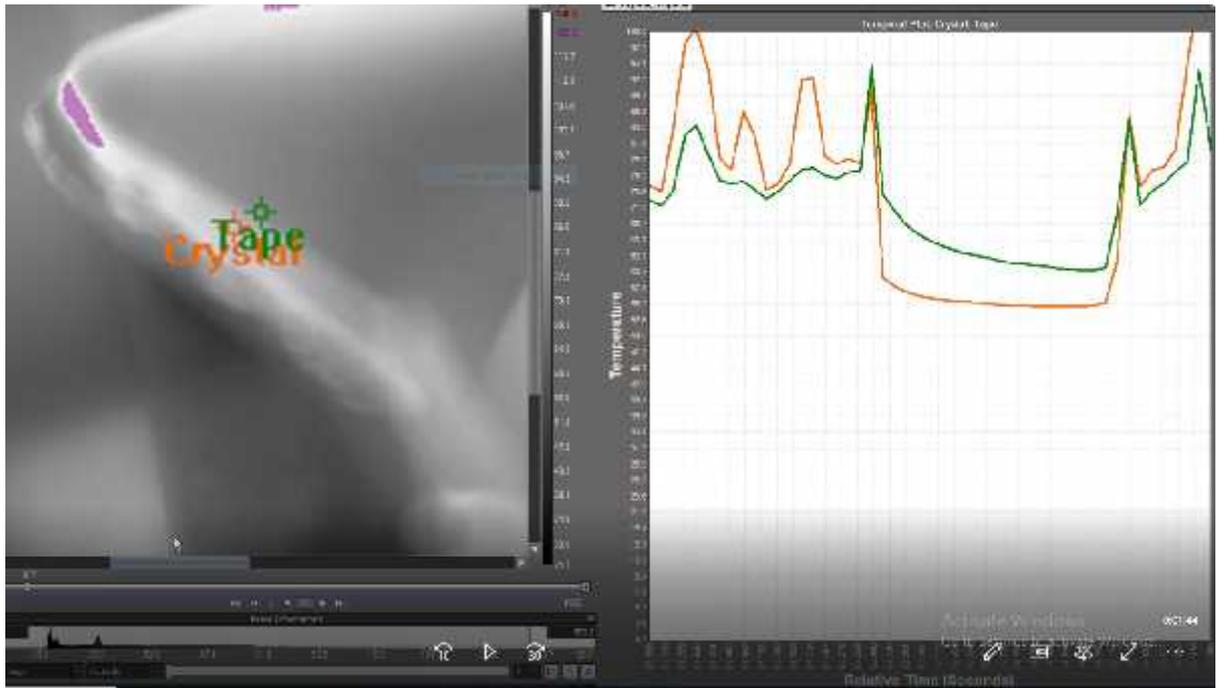
Figure 31 Intensity of detected signal (temperature) for crystal & tape measured by radiation thermometer (at the beginning of heat transfer).

The difference of the information density can be clearly noticed
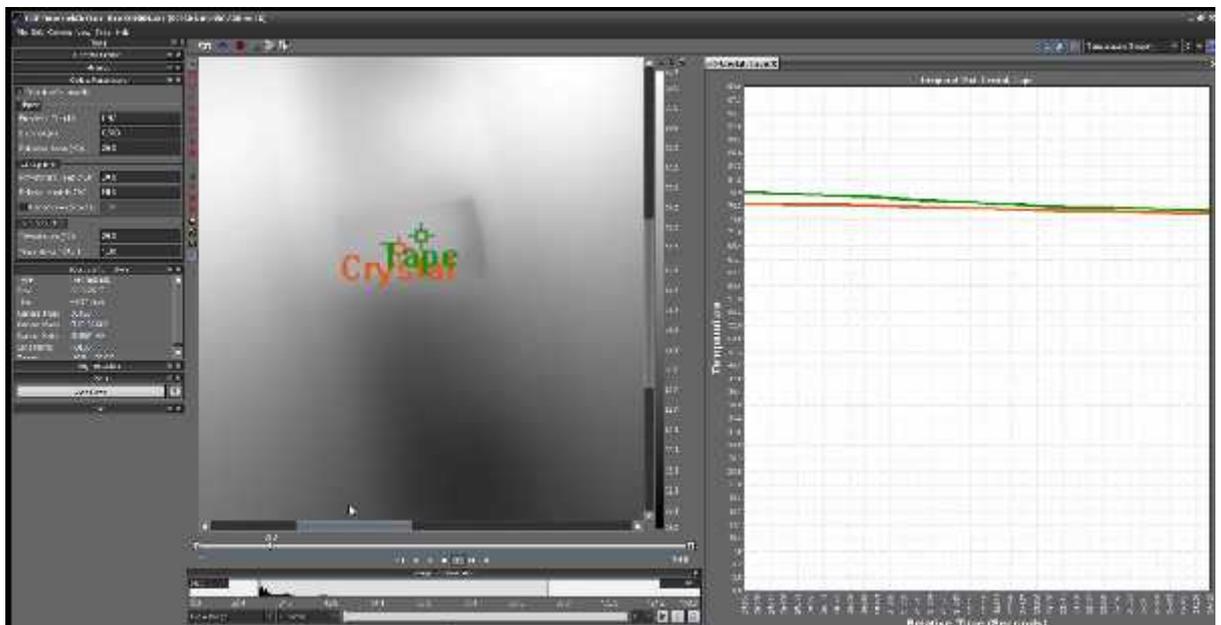
Figure 32 Intensity of detected signal (temperature) for crystal & tape, measured by radiation thermometer (at Thermal equilibrium).

The difference of the thermal information almost zero

6.3.1. Setup for calibration of the radiation thermometer using the infrared camera

An IR thermometer can be compared to the human eye. The lens of the eye represents the optics through which the radiation (flow of photons) from the object reaches the photosensitive layer (retina) via the atmosphere. This is converted into a signal that is sent to the brain. Fig. 33 shows an infrared measuring system process flow.
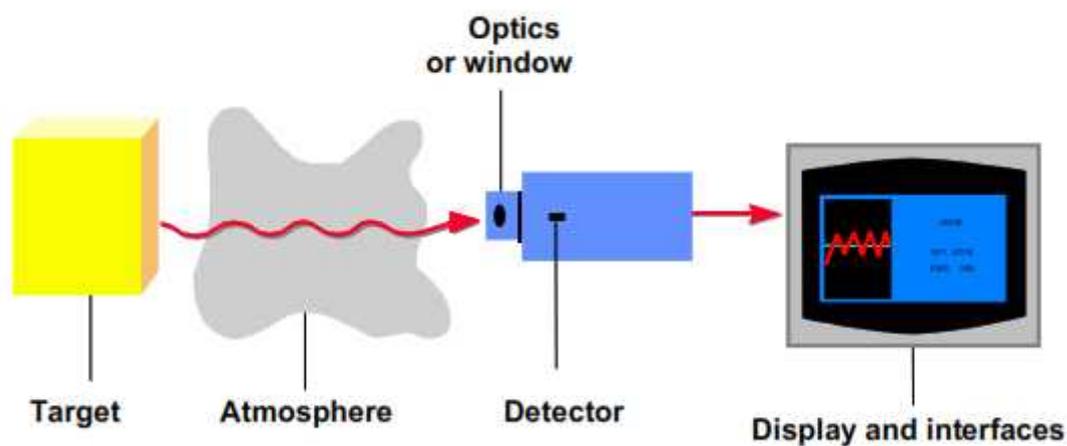
Figure 33 Calibration of the radiation thermometer

6.4. Verification of the temperature measurement method

It is possible to measure the temperature of the crystal by measuring $\Delta\theta_0$ by Δ / Σ at the moment when the magnetic field induction is zero. There are two such points per period, and further averaging is also possible since the temperature changes slowly. This makes this method inherently capable of good signal-to-noise ratios since averaging the temperature at, say, 100 points (2 points per period, 50 period per second, and 1 reading of temperature per second) significantly improves the SNR.

After the determination of temperature, it is possible to calculate V(T), and this eliminates the temperature influence on the sensor transfer function. In other words the temperature can be calculated as

$$T = T(\theta_0) \tag{6.1}$$

Once the temperature of the crystal sample is determined, it is possible to compensate the current measurement and obtain the compensated measured current as

$$I_c = V\big(B, T(\theta_0)\big) = \frac{V(T_0)}{V(T)} I(T) \tag{6.2}$$

In order to calculate the temperature of the crystal sample, it is necessary to know the optical activity of the crystal versus temperature. The temperature dependence of the $B_1 G O_2$ optical activity was measured, and the reported value is 0.0001 rad/mmK = 0.00573 deg/mmK. It is possible to construct a setup that would simultaneously measure the optical activity and the Verdet constant against temperature and thus calibrate the sensor transfer function. Thus, with knowledge of the temperature dependence of both the optical activity of the crystal and the Verdet constant, it is possible to calculate the Faraday crystal sample temperature, calculate V(T), and adjust (compensate) the calculated current to make it temperature-insensitive [31].

6.5.   Radiation thermometer characteristics

A solid understanding of infrared technology and its principles lies behind accurate temperature measurement. When the temperature is measured by a noncontact device, the IR energy emitted from the measured object passes through the optical system of the thermometer and is converted to an electrical signal at the detector. This signal is then displayed as a temperature reading. There are several important factors that determine accurate measurement. The most important factors are emissivity, distance-to-spot ratio, field-of-view, and location of a hot spot [33].

6.5.1. Emissivity

All objects reflect, transmit, and emit energy. Only the emitted energy indicates the temperature of the object. When IR thermometers measure the surface temperature they sense all three types of energy, therefore all thermometers have to be adjusted to read emitted energy only. Measuring errors are often caused by infrared (IR) energy being reflected by light sources. Some IR thermometers allow you to change the emissivity in the unit. The value of emissivity for various materials can be looked up in published emissivity tables. Other units have a fixed, preset emissivity of 0.95, which is the emissivity value for most organic materials and painted or oxidized surfaces. If you are using a thermometer with a fixed emissivity to measure the surface temperature of a shiny object, you can compensate by covering the surface to be measured with masking tape or flat black paint. Allow time for the tape or paint to reach the same temperature as the material underneath. Measure the temperature of the taped or painted surface. That is the true temperature.

6.5.2. Distance-to-spot ratio

The optical system of an infrared thermometer collects the infrared energy from a circular measurement spot and focuses it on the detector. Optical resolution is defined by the ratio of the distance from instrument to the object compared to the size of the spot (90% of energy) being measured (DSR). The larger the ratio number the better the instrument's resolution, and the smaller the spot size that can be measured.

The laser sighting included in some instruments only helps to aim at the measured spot. A recent innovation in infrared optics is the addition of a Close Focus feature, which provides accurate measurement of small target areas without including unwanted background temperatures.

6.5.3. Field-of-view (FOV)

Make sure that the target is larger than the spot size the unit is measuring. The smaller the target, the closer you should be to it. When accuracy is critical, make sure that the target is at least twice as large as the spot size.
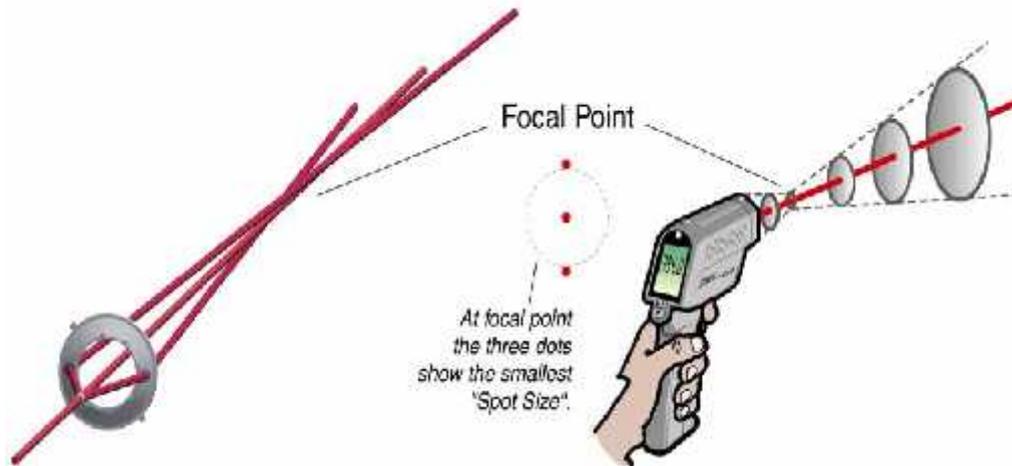
Figure 34 Measured target temperature & field of view

6.5.4. Radiation thermometer Specifications

In table shown below we can see the specification of radiation thermometer used in the experiments [33].

Table 4 Radiation thermometer Specifications

Distance To Target Size Ratio	(D:S)50:1
Emissivity	Adjustable
Sighting	Type3-point laser
Laser Class	Class II
Min Temperature (° F)	-25
Max Temperature (° F)	1600
Min Temperature (° C)	-30
Max Temperature (° C)	900
Accuracy	±0.75% reading or ±2.0°F (±1.0°C), whichever is greater
Resolution	0.2°F (0.1°C)
RS-232 Interface	Yes
Battery	AA Battery (2)
Description Model	Noncontact Infrared Thermometer with Digital Photography, Close Focus

Specification for the green laser used in experiments is obtained from [34].

Table 5 Green Laser Specification

Model	GLM-5
Power 1 – 3 mW 3 – 5 mW	5 – 10 mW
Wavelength	532nm
Power	5 – 10 mW
Output Mode	CW (continuous wave) + modulation (DC – 10kHz, digital)
Operating Voltage	9V
Operating Current	< 400mA
Beam Divergence	< 1.4 mrad
Dimension	20 x 50 mm
Operating Temperature	25~30 °C

7. Measuring of the optical activity and Verdet constant

7.1. Setup for measurement of optical activity against wavelength and temperature

Faraday crystal ($B_1 G O_2$) is next in the optical path causing rotation of the polarization plane due to its own temperature-dependent optical activity and the temperature-dependent Faraday effect.

The magnetic field is created by Helmholtz coils (HC) powered from an AC current source with a reference ampermeter connected in series. The relation between the magnetic induction in the coil center and the coil current (I) is known; thus, it is possible to measure the Verdet constant.

CaCO3 is used as a beam splitter producing two coaxial beams with polarization planes set 90 ∘ apart. The intensities of the two beams emerging from the BS are sensed using two quadrants from four quadrant photodiodes (QPDs). This is preferred to two individual photodiodes since the quadrants on a quadrant photodiode are more closely matched in responsivity. The photocurrents from the diodes are amplified with transimpedance amplifiers (DUAL TIA) and sampled using a 16-bit dual ADC. The results are relayed to a PC over a USB interface and using a FIFO to prevent data loss. An electronic processing unit (ECB) is encased in a Faraday cage to minimize EMI effects. The temperature of the crystal is controlled by placing the HC and the crystal in an enclosed chamber with temperature control. The chamber is depicted as a gray area in the picture. The chamber contains a temperature measurement unit (Radiation thermometer) for monitoring the crystal temperature [35].
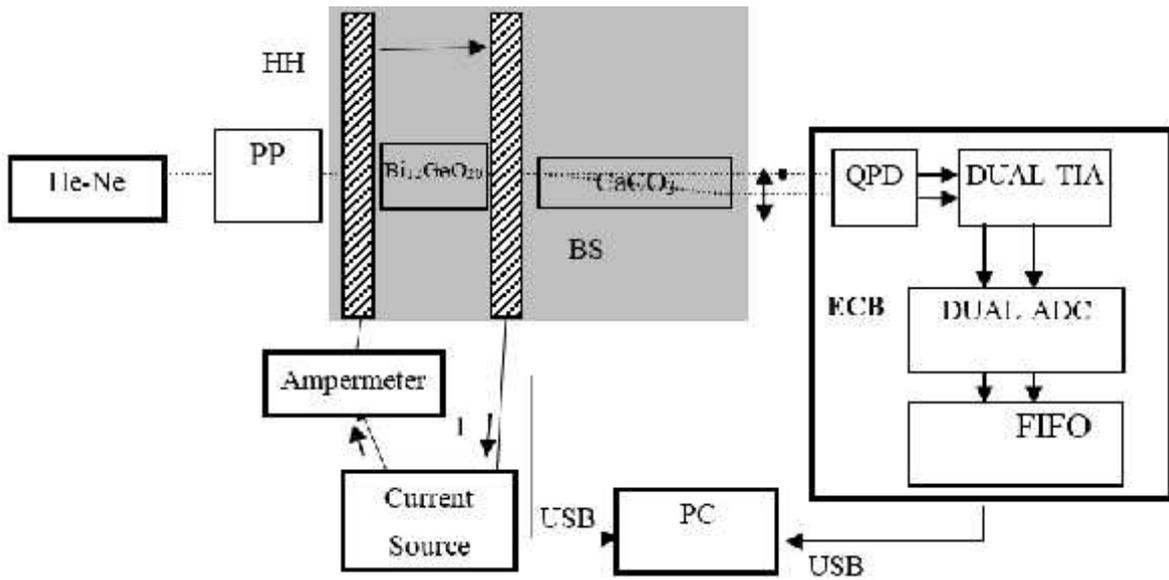
Figure 35 Optical Activity Setup

Figure 36 The mounting setup used to suspend the crystal in the Helmholtz coils magnetic field.

Figure 37 Polarizing prism.

In the presence of a magnetic field the rotation angle (φ) of the polarization plane of linearly polarized light by the Faraday crystal can be calculate using the experiment setup shown (Figure 38).

Figure 38 The crystal and the beam splitter mounting setup.

7.2.   Measuring of the Verdet constant

The Verdet constant is a measure of how strong the Faraday Effect is in a particular material. The Verdet constant is also wavelength dependent and will be affected by temperature. In order to keep high sensitivity for the sensor a stable Verdet constant is required which in turn will put certain requirement on both the material and the wavelength of operation.

The Verdet constant is calculated from

$$V = \frac{\Theta_A}{B_0 l} = \frac{1}{2 B_0 l} \sin^{-1} \left[\frac{U_1 - U_2}{U_1 + U_2} \right]_{\Theta_A}$$

(7.1)

where Θ_{AC} is the amplitude of the AC signal, B_0 is the amplitude of the magnetic induction, whereas U_1 and U_2, are the output signal voltages obtained after transimpedance stages from the vertically and horizontally polarized components, respectively. The FFT was used to separate spectral components of U_1 and U_2. The Faraday rotation was determined from the magnitude of the 50 Hz component. The absorption coefficients were obtained by measuring the difference in beam intensities at the quadrant photodiode[36] with and without BGO crystal in the beam path. The reflection on the BGO crystal was calculated using the normal incidence and BGO refraction index of BGO, n = 2.55. The absorption coefficient, α, was calculated from the beam intensities with and without the crystal present in the beam path, I(x) and I(0), and the known crystal length l = 9.8 mm as

$$I(l) = I_0 e^{-\alpha l} \quad \longrightarrow \quad \alpha = -\frac{1}{l} \ln \frac{I(l)}{I_0}$$

(7.2)

The magneto-optical quality is calculated by dividing the Verdet constant by the absorption coefficient. The obtained results are given in Table 6

Table 6 Magneto-optical properties of irradiated and unirradiated high purity crystal samples

Property	Unirradiated sample	Irradiated sample
Verdet constant (rad $T^{-1}m^{-1}$)	72	72
Absorption coefficient (cm^{-1})	0.58	0,34
Magneto-optical quality (rad T^{-1})	1.24	2.1

The data given in Table 6 show the effects of femtosecond laser irradiation on the magneto-optical properties of the high purity BGO crystal. The irradiation caused 41.4% decrease in the absorption coefficient and did not influence the Faraday constant. Consequently, the increase in crystal transparency resulted in a significant 70% increase in the magneto-optical quality. As explained earlier, increase in crystal transparency is an important gain from the point of view of a sensor system since the system-level signal-to-noise ratio is directly proportional to the magneto-optical quality of a crystal. Therefore, it is expected that the signal-to-noise ratio of a sensor system would be improved by the same amount as the improvement in the magneto-optical quality induced by the irradiation. Consequently, it can be concluded that the femtosecond pulsed laser irradiation affects the crystal in a positive manner.

7.3.   Wavelength dependence of the Verdet constant

Early quantum mechanical considerations of visible and ultraviolet light propagating through gaseous materials predicted a Verdet constant that varies approximately as the square of the frequency, where v $1/\lambda$. Generally, the Faraday Effect description reflected H. Becquerel's derived classical expression for the Verdet constant,

$$V = \frac{\omega(n_- n_+)}{2c_i} = \left(e / 2m \right)^d / d$$

(7.3)

which shows that V is proportional to the dispersion, d / d . This describes a change in the index of refraction as a function of wavelength, where, in the long wavelength regime, as shown in Figure 39 , The Verdet constant is inversely proportional to the wavelength squared, $1/\lambda^2$ [37].
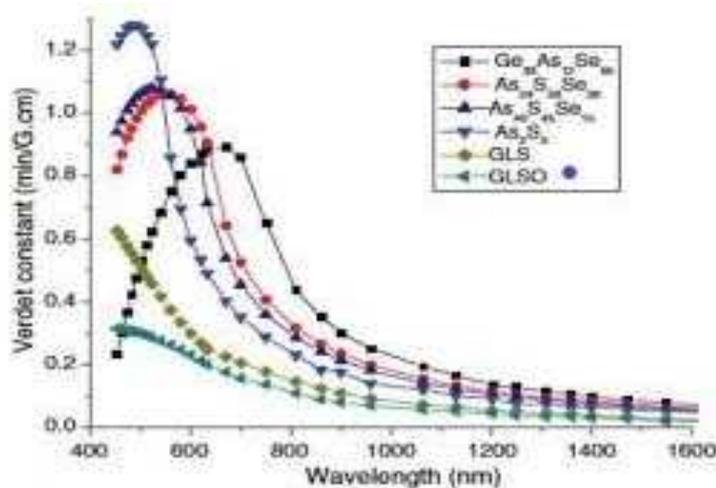
Figure 39 The Verdet constant for various materials as a function of the wavelength [38].

This behavior as understood in terms of the atomic vector polarizability is given by:

$$a_v = \frac{2\omega r_e c^2}{} \sum_k \frac{f_k a_k}{(\omega_k^2 - \omega^2)^2}$$

(7.4)

Where r_e is the classical electron radius, ω is the frequency of the incident light, and the sum is taken over the dipole transition allowed excited states with resonance frequencies ω_k , oscillator strengths f_k and hyperfine coupling constants are given by $H_k^{hf} = a_k \vec{L} = \vec{I}$ in which the angular momentum quantum number is L and I is the nuclear spin of the atom[39].

7.4. Temperature dependence of the Verdet constant

The magnets and the Faraday rotator materials both exhibit a temperature dependence. Both the magnetic field strength and the Verdet Constant decrease with increased temperature. For operation greater than ±10 °C beyond room temperature, there are always requirements on accuracy when doing measurements. Furthermore, there also may be requirements of keeping the accuracy even if the temperature is changing. In electrical substations, sensors needs to keep an accuracy of ±0.2%[40] with temperature ranging from −40∘C to 85∘C. Fiber optic current sensors have in the past experienced high sensitivity to temperature, which have limited the performance severely. The main reason for this is that temperature changes result in stress-induced linear birefringence in the sensing coil of the sensor[41]. Even though several techniques have been proposed in order to increase the performance, there is still the matter of the inherent temperature dependence of the Verdet constant.

7.5. Experimental Results

Table 7 Results of absorptions and Rotations of plane polarization of crystals due to magnetic field using experiment setup shown in Figure 35

Crystal Type	Current [A]	Rotation [deg]	Absorption - with crystal	Absorption - without crystal	Crystal length [mm]
Reference Crystal	4,14	0,62	0,316	0,78	10
Z11	4,14	0,62	0,404		9,9
C11	4,14	0,315	0,065		9,7
C12	4,14	0,395	0,083		9,7
C13	4,14	0,502	0,11		9,6
C14	4,14	0,514	0,099		9,54
Background level			0,065		
Temperature 24 [deg]					

Table 8 Results of Verdet constant (V)& Magneto Optical Quality (MOQ), for different samples of crystals.

Sample	Current[A]	Length [m]	Rotation [deg]	Rotation [rad]	Magnetic field [T]	Verdet const [rad/mT]	MOQ [rad/T]
Reference crystal	4.14	0.01	0.62	0.0108	0.0053	203.77	2.04
Z11	4.14	0.0099	0.62	0.0108	0.0053	205.83	2.04
C11	4.14	0.0097	0.315	0.0055	0.0053	106.98	1.04
C12	4.14	0.0097	0.395	0.0069	0.0053	134.22	1.30
C13	4.14	0.0096	0.502	0.0088	0.0053	172.96	1.66
C14	4.14	0.00954	0.514	0.0090	0.0053	178.00	1.70

The Magneto optical quality (MOQ), of reference crystal and the crystal Z11 are same, although their Verdet constants are nearly same that is supposed to be happened because the small difference in their lengths.

For other crystals samples, (C11, C12, C13& C14), we can see from the results that the proportionality between the Magneto optical quality and the Verdet constant.

7.6. Setup for measurement of Verdet constant against wavelength and temperature
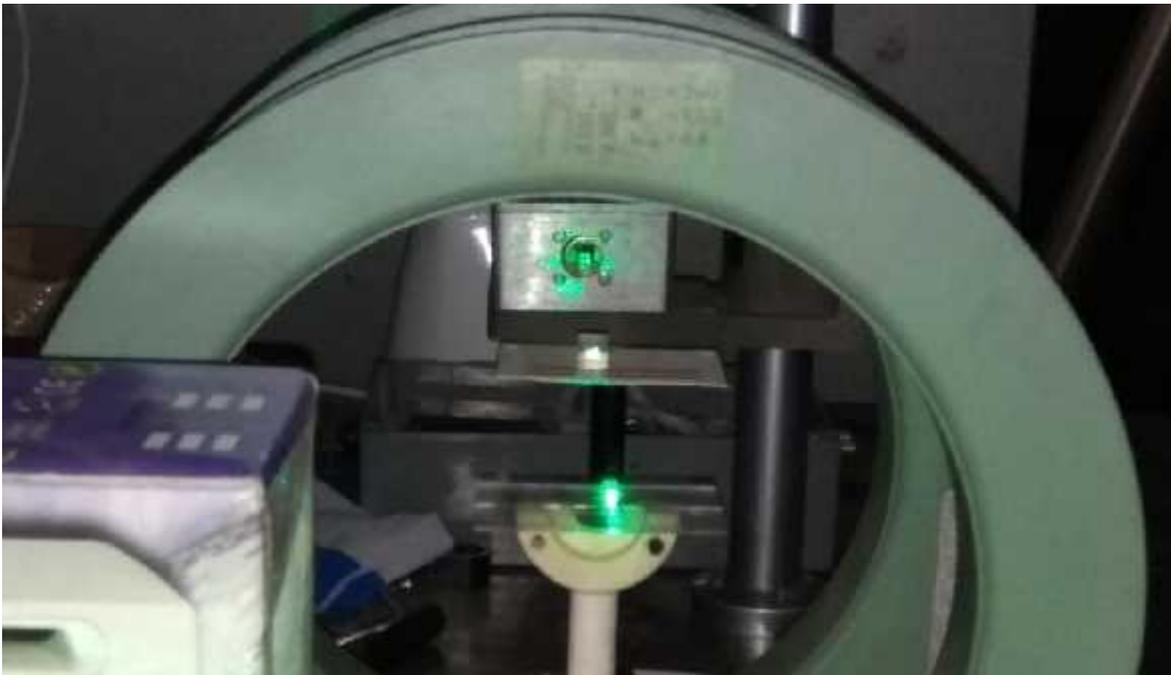
Figure 40 The beam path – the crystal followed by the beam splitter and photodetector.

To achieve the two polarized light beams we have used calcite (CaCO3). After the light (laser beam) passing through the calcite (CaCO3), will spatially divide the laser beam into components ordinary and extraordinary rays.

Figure 41 Beam splitter action on the polarized green laser beam following optically active crystal.

Figure 42 Laser beam spots on the photodiode detector following the beam splitting process.

7.7. Effects of laser irradiation on the BiGeO crystal

The equipment used to produce the femtosecond pulsed laser beam and establish its wavelength was the Coherent Mira 900F femtosecond laser, Coherent Verdi V-10 pump laser that provided a 532 nm continuous wave pump beam, and Ocean Optics HR2000CG UV-NIR spectrometer. Crystal samples were irradiated along the crystal growth direction (z), i.e. along the samples' longest axis. The irradiating laser beam radius provided partial irradiation of the exposed crystal facet. The beam wavelength was 800 nm, whereas its power was increased from 50 mW to 950 mW and was adjusted by a graded filter. The pulses were 90 fs long and had repetition rate of 76 MHz The samples were irradiated by each beam power for 3 s. The beam power was measured with the Ophir power meter with the thermal and photometric heads. In order to enable comparison of the irradiation effects on the single crystal samples of different purity, i.e., on yellow and black $Bi_{12}GeO_{20}$ samples, the irradiation conditions were intentionally chosen to be identical to those applied to the lower purity black crystals in[1]. The sample color was calculated from the transmission spectra measured by the Beckman Coulter DU 720 General Purpose UV/VIS spectrometer.

7.7.1. Transmission spectra

The irradiation pattern applied here to the higher purity yellow crystals is identical to the one utilized in [2] to irradiate black crystals grown from the components of lesser purity. Consequently, the obtained results can be compared and the differences can be attributed solely to different sample purity. With the increase of irradiating laser power, the transmittance of irradiated sample undergoes initial growth followed by a decrease, as can be seen in Figure 43 Comparison with the dependence corresponding to the black crystal given in[1] reveals that the transmittance curves for the black as well as for the yellow crystal has the same shape and that the slopes of the two curves appear to be approximately equal. The curve corresponding to the yellow crystal is shifted to

the larger values by approximately 18.8% compared to the curve corresponding to the black crystal. For the yellow crystal, the maximal transmittance of 44.0% occurs at the irradiating laser power of 451 mW, whereas the lower purity black crystal was reported in [1] to have the smaller maximal transmittance value of 25.1% corresponding to 455 mW. It seems that both curves exhibit local irregularities which occur at 197.4–249.7 mW, 552–605 mW and 800–857 mW for the black crystal and at 593–641 mW for the yellow crystal. It is possible that the irregularity in the yellow sample curve for large values of incident power P_0 is not visible because it is outside the considered range of irradiating laser power, or due to insufficient measurement accuracy achieved for yellow crystal data points above 700 mW.
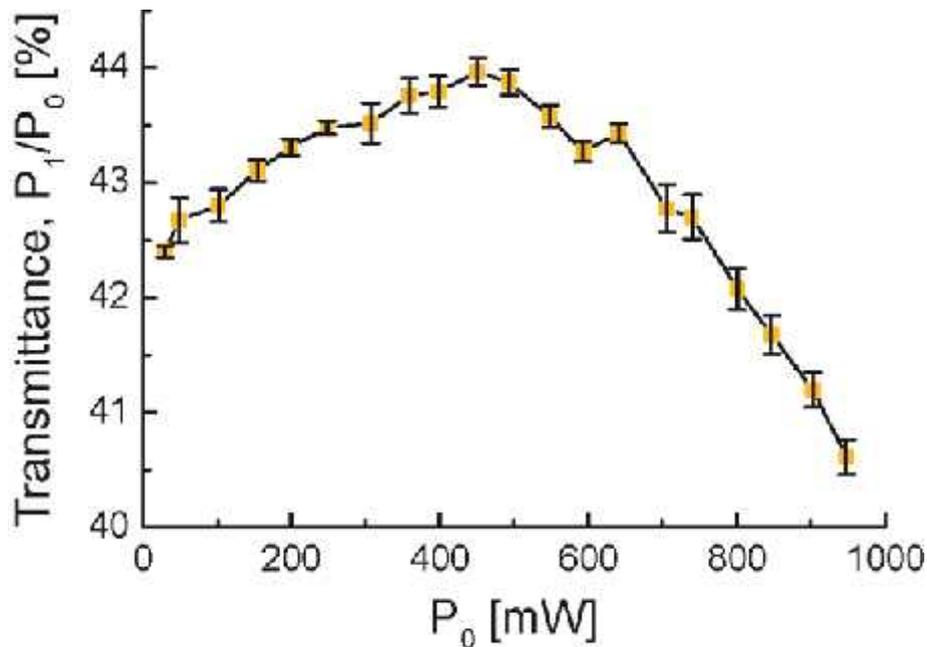
Figure 43 Change of crystal transmittance with increase of irradiating laser power

For each value of the incident power P_0, a sample is irradiated by the femtosecond laser beam for 3s. The transmittance is given as P_1 / P_0, where P_1 is the transmitted power. The error bars were calculated from the uncertainties of measured values of the incident and transmitted power, ΔP_0 and ΔP_1.

Transmission spectra of samples were determined along both directions of the longest sample axis and are shown in Figure 44 . In addition to the treated samples, i.e., the samples irradiated by the femtosecond laser beam of increasing power, the unirradiated samples were examined, as well. The unirradiated crystal exhibits noticeable anisotropy. The transmissions of the crystal have small irregularities, which are probably caused by impurities, at 655 nm and 800 nm and a steep growth after 850 nm. For the unirradiated crystal the transmission corresponding to the z direction is larger than the one in the -z direction. For wavelengths larger than 1000 nm the transmission is larger than 37 % and 24 % in the z and -z direction, respectively. After irradiation the anisotropy disappeared, and the transmission of the crystal increased becoming larger than 51 % for wavelengths above 1000 nm. Measurements repeated after prolonged period of time confirmed full reproducibility of the obtained results and verified that the detected light- induced changes are permanent [1].
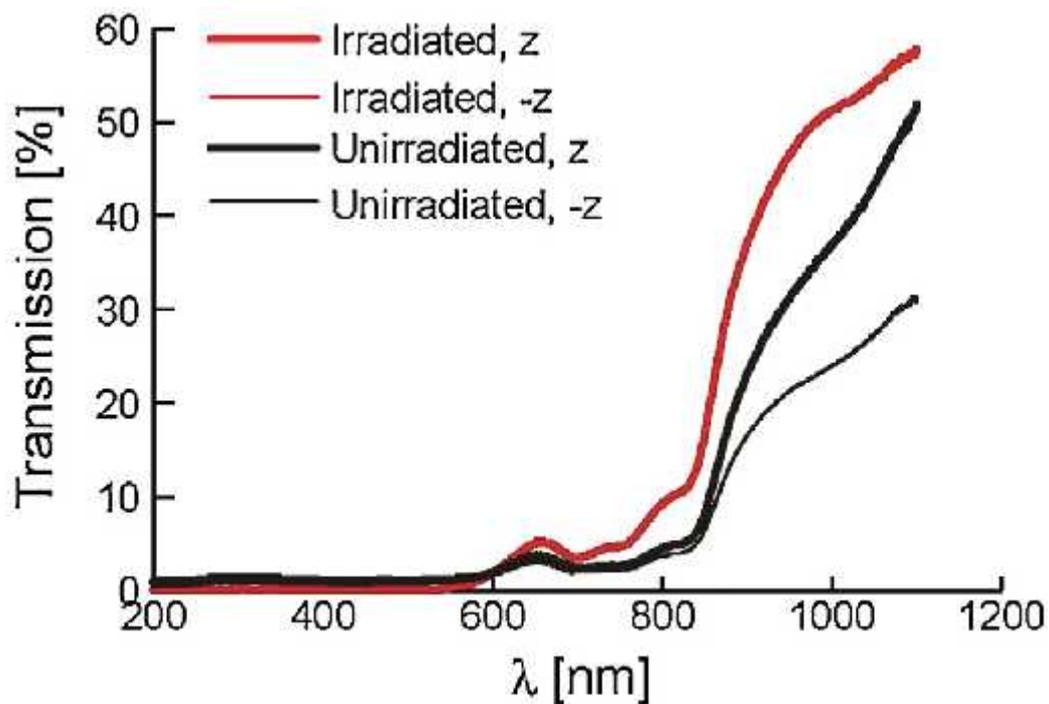
Figure 44 Transmission spectra of irradiated and unirradiated samples

The transmission spectra of all samples were measured in the direction of crystal growth as well as in the direction opposite to it. The unirradiated sample

exhibits significant anisotropy, which disappears after irradiation. Irradiation also causes transmission increase.

7.7.2. Chromacity diagram

The change of Bismuth Germanium oxide single crystal ($Bi_{12}GeO_{20}$) color caused by irradiation was noticeable to the naked eye. It was calculated from the transmission spectra measured by the Beckman Coulter DU 720 General Purpose UV/VIS spectrometer [2].
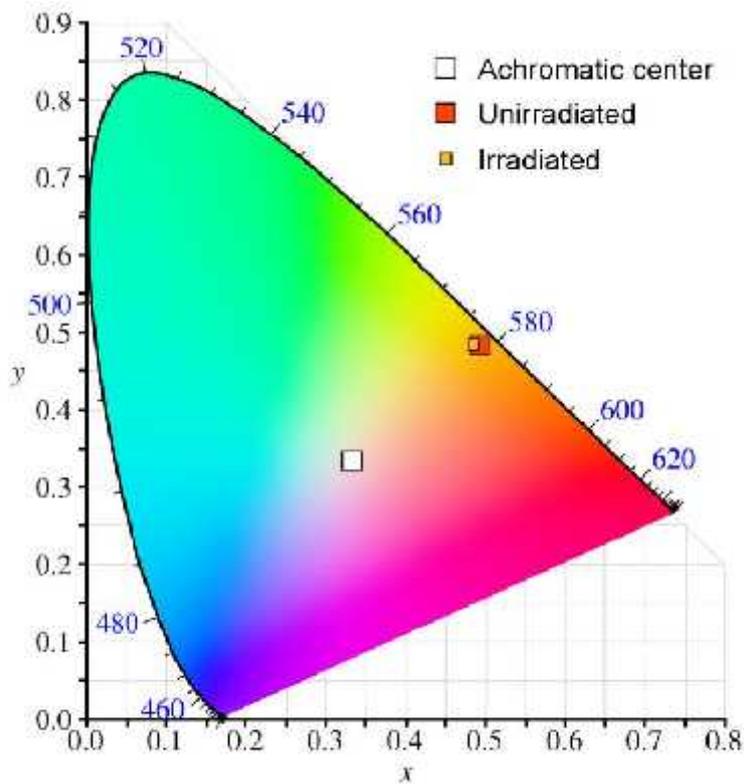
Figure 45 Sample colors in CIE chromaticity diagram.
The change in the crystal color was visible to the naked eye [2].

7.7.3. X-ray spectra

The X-ray diffraction patterns were measured with the Rigaku Ultima IV Multipurpose X-ray diffraction system. The system was operated at 40 kV and 40 mA to produce nickel-filtered CuK a 1 X-ray with l = 0.1540 nm. The XRD data

were collected in the 2 u range between 20 and 70 at the scanning rate of 5 1/min. The phase analysis was performed using the PDXL2 software, version 2.0.3.0[42].

7.7.4. Raman spectra

The Raman spectra of unirradiated and irradiated samples are recorded at room temperature in the spectral range from 150 to 800 cm^{-1} and are shown in Figure 46 The results obtained for unirradiated crystals are in agreement with those given in[1] After irradiation the intensity of the F(TO) peak at 203 cm^{-1} decreased, whereas all other peaks became more pronounced. Despite the difference in purity between the yellow samples studied here and the black crystals considered in[36] the Raman spectra of unirradiated crystals do not differ significantly. As reported in [36], irradiation of the black crystal caused all the peaks of symmetry type E, i.e., the peaks at 234, 454, and 619.6 cm^{-1} , to disappear and intensity increase of all other peaks. The change in the same Raman spectrum peaks of

$Bi_{12}GeO_{20}$ was reported in[22]; however, the most, medium, and least intense peaks correspond to the annealed, doped, and untreated samples, respectively.
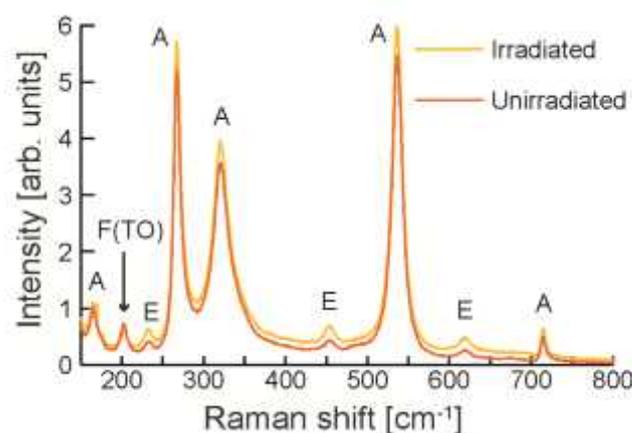
Figure 46 Raman spectra. Irradiation caused a small upward shift of the crystal spectrum except for the F(TO) type peak at 203cm^{-1}

8. Results and discussions

This section will present results obtained in experiments in application perspective trying to correlate experimental data with engineering application.

8.1. Optical activity of the BiGeO crystal with respect to temperature

Temperature dependence of the change of optical activity of the BiGeO crystal from set point obtained by experiments described in chapter 7 is shown in the Figure 47. Difference in the variation of optical activity versus temperature of the crystal and the laser wavelength implies not only that the wavelength is an important factor in the design of a non-reflective configuration for a magnetic field sensor but also opens a possibility to detect the crystal temperature using wavelength multiplexing.
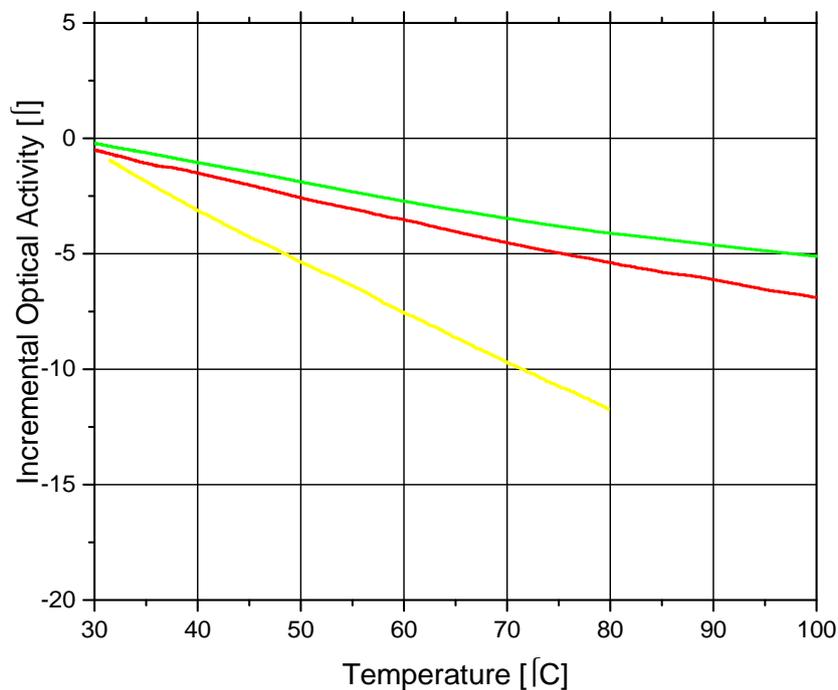
Figure 47 BiGeO change of optical activity versus temperature.

For a single wavelength excitation in a transmissive configuration temperature will affect the rotation of the plane of polarization due to its effect on optical

activity. Within a range of temperatures that were measured the shift will range from 5° up to 12° regardless of the magnetic field in the crystal. If a Δ/Σ method is used to determine plane of polarization rotation (θ) this shift will be detected and could create false indication of the magnetic field intensity change. Given small values of Verdet constant for a BiGeO crystal and small crystal lengths of few millimeters, optical activity temperature shift can easily mask the measurement. This issue is further complicated by the fact that temperature frequency spectra is close to DC thus preventing the magnetic field intensity measurement by frequency separation in the spectrum. Such an error is not acceptable and cannot be eliminated by calibration. In addition to creating an issue in Δ/Σ configuration, optical activity creates equal concern in an AC/DC normalization scheme. Verdet constant of the BiGeO crystal with respect to temperature. Variation of the Verdet constant with temperature is shown in

Figure 48 (experiments from chapter 7) that demonstrates that Verdet constant decreases with increasing temperatures. A typical BiGeO crystal exhibits 0.5°/T/mm decrease in Verdet constant on a 30°C-70°C temperature range.
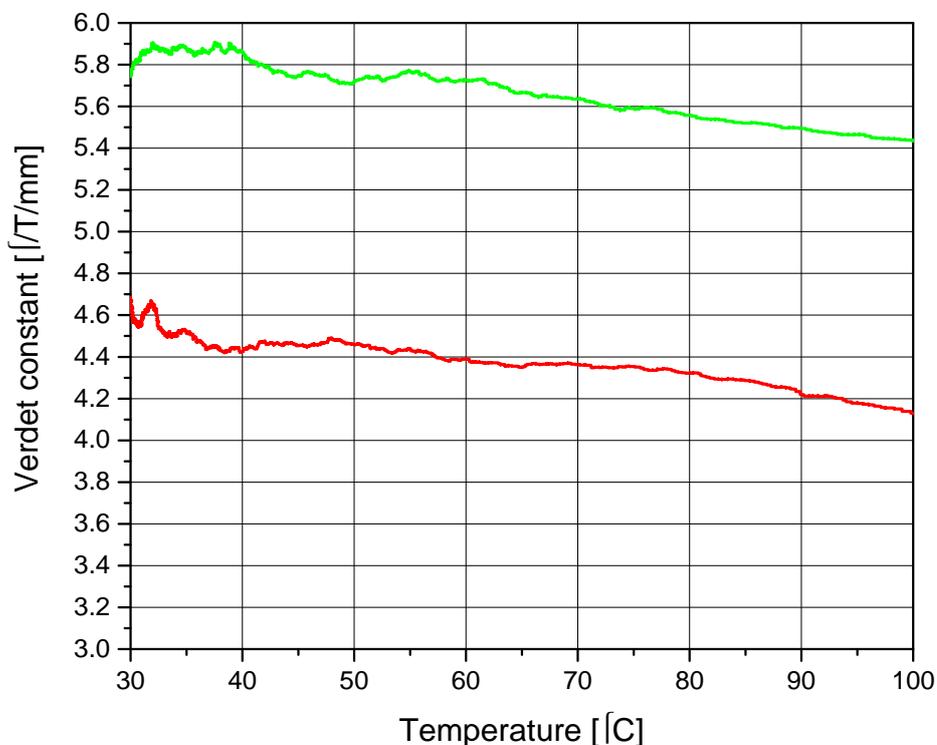
Figure 48 BiGeO Verdet constant versus temperature.

This change in Verdet constant is the chief reason that causes the optical magnetic field or current sensors to show temperature dependent error, since value of magnetic field intensity is usually calculated from

$$B(T) = \frac{\theta}{V(T)l(T)}$$
(8.1)

Since crystals expand thermally, crystal length l is also a function of temperature, but the coefficient of thermal expansion of a BGO crystal is small with the value of a = 16.8 $\cdot 10^{-6}$ K^{-1} thus making $l(T)$ change negligible [27]. This change is actually welcome, since increasing l with temperature compensates a little for decreasing V with temperature, but insufficiently.

In a general case, rotation of the plane of polarization θ is caused by both the Faraday Effect and optical activity

$$\theta(T) = \theta_F(T) + \theta_O(T)$$
(8.2)

Aside from crystal expansion, when a crystal is subjected to temperature change at least three additional variations take place:

1. Verdet constant changes with temperature $\theta_F(T)$

2. Optical activity varies with temperature $\theta_{OA}(T)$

3. Light source wavelength shift with temperature $\lambda(T)$

In a general case one can write

$$\frac{d_{"}}{dT} X_{"F} \frac{1}{V} \frac{|V\ d\}}{|\}\ dT} \Gamma \frac{|V}{|T} \Gamma \frac{1}{l} \frac{|l}{|T} \Gamma \frac{d_{"OA}}{dT}$$
(8.3)

with various terms having different values depending on the sensor configuration. Also, in a serious sensor design light source temperature is regulated in such a manner so as to preserve the wavelength, i.e. wavelength shift with temperature is negligible. Having this in mind and negligible crystal expansion for a transmissive configuration Eq. (*8.3*) can be simplified to

$$\frac{d_{\shortmid}}{dT} \, \mathrm{X}_{\shortmid F} \, \frac{1}{V} \, \frac{|V}{|T} \, \Gamma \frac{d_{\shortmid OA}}{dT} \tag{8.4}$$

However, for a reflective configuration Eq. (8.4) is further simplified to

$$\frac{d_{\shortmid}}{dT} \, \mathrm{X}_{\shortmid F} \, \frac{1}{V} \, \frac{|V}{|T} \tag{8.5}$$

since optical activity cancels out.

One can now appreciate the reasons for measuring Verdet constant variation with temperature and optical activity shift with temperature when assessment of temperature variation effect on Faraday magnetic field sensor is considered.

To address this issue it is possible to use at least two different wavelengths for measuring magnetic field intensity and then use these results to correlate which part of the plane of polarization rotation is caused by temperature and by magnetic field. Due to difference in normalization, temperature compensation is performed differently and accordingly shall be discussed separately.

8.2. Temperature Compensation with AC/DC Normalization

A typical AC/DC configuration would have a linearized transfer function defined as

$$U_L \, \mathrm{X} \frac{U_0}{2} f 1 \, \Gamma \cos 2_{\shortmid 0} \, \Gamma 2_{\shortmid} \, \sin 2_{\shortmid 0} A \tag{8.6}$$

where θ_0 is rotation of the plane of polarization due to DC magnetic field, optical activity and construction induced phase shift, θ is rotation of the plane due to magnetic field only, U_0 is detector output voltage at zero magnetic field. θ_0 is usually set to 45° by customizing transmission axis of polarizer and analyzer to obtain maximum sensitivity (sin(90°)=1). Shift in θ_0 due to temperature will affect the measured DC value of U_L from second term in the sum and the AC

value of the measured magnetic field from the third term in the sum. Since AC/DC normalization operates by dividing the AC part of the U_L with its DC part resulting variation of the U_L caused by temperature shift of the optical activity is a serious problem.

When Eq. (8.6) is split into its DC and AC part one obtains

$$U_{LDC} \approx \frac{U_0}{2} fl\Gamma \cos 2\theta_0 A$$

$$U_{LAC} \approx U_{0''} \sin 2\theta_0$$

(8.7)

When AC/DC normalization is applied using previous equations one obtains a number N_{ACDC}

$$N_{ACDC} \approx \frac{U_{LAC}}{U_{LDC}} \approx \frac{U_{0''} \sin 2\theta_0}{\frac{U_0}{2} fl\Gamma \cos 2\theta_0 A} \approx \frac{2\sin 2\theta_0}{l\Gamma \cos 2\theta_0}$$

(8.8)

from which magnetic field intensity θ can be obtained as

$$B \approx \frac{1}{2Vl} \frac{l\Gamma \cos 2\theta_0}{\sin 2\theta_0} N_{ACDC} \approx k fT N_{ACDC}$$

(8.9)

Since V and θ_0 are both functions of temperature the result for B will also depend on temperature even when magnetic induction is constant since scale factor k is temperature dependent.

$$\frac{\partial}{\partial} = \frac{\partial \left(\frac{1}{2V} \frac{1+c \ 2\theta_0}{s \ 2\theta_0} \right)}{\partial}$$

(8.10)

Calculation of the first derivative of Eq. (8.10) takes some steps:

$$\frac{\partial \left(\frac{1}{2V} \right)}{\partial} = -\frac{1}{2V^2 l} \frac{\partial}{\partial}$$

,

$$\frac{\partial \left(\frac{1+c \ 2\theta_0}{s \ 2\theta_0} \right)}{\partial} = = \frac{-2s \ ^2 2\theta_0 - 2c \ 2\theta_0 - 2c \ ^2 2\theta_0}{s \ ^2 2\theta_0}$$

(8.11)

Thus it is possible to obtain temperature derivative of the scale factor k

$$\frac{\partial}{\partial} = -\frac{1}{2V^2 l}\frac{1 + c_i\ 2\theta_0}{s_i\ 2\theta_0}\frac{\partial}{\partial}$$
$$+ \frac{1}{2V}\frac{-2s_i^2 2\theta_0 - 2c_i\ 2\theta_0 - 2c_i^2 2\theta_0}{s_i^2 2\theta_0}\frac{\partial\theta_0}{\partial} \tag{8.12}$$

Since θ_0 is set to 45° to obtain maximum sensitivity one can further reduce to

$$\left.\frac{|k|}{|T|}\right|_{\theta_0 \times 45^\circ} X Z \frac{1}{2V^2 l}\frac{|V|}{|T|} Z \frac{1}{Vl}\frac{l_{\theta_0}}{|T|} \tag{8.13}$$

Given negative values of temperature changes for V, noting that V is smaller than 1 (in S.I. unit for V is rad/T/m) and that temperature affects Faraday effect and optical activity with similar scale, second term can be neglected causing the sensor scale to rise with temperature.

Thus in an AC/DC normalization system of primary concern is the scale change of the sensor due to temperature effect on Faraday constant and to compensate one must obtain accurate value of V at the crystal temperature.

There are several solutions available but the one option possible using data obtained in this thesis is to measure the magnetic field strength at two wavelengths λ_1, λ_2 and the find the crystal temperature using their relation. Thus since V is also a function of λ one obtains

$$B_1\ X k f\}_1, T\ A N_{ACDC1}, B_2\ X k f\}_2, T\ A N_{ACDC2} \tag{8.14}$$

However, by close examination of $V(T, \lambda)$ graphs it is noticeable that the $V(\lambda_1)$ and $V(\lambda_2)$ are similar, they both decrease in the same manner and maintain constant ratio. This makes compensation impractical.

8.3. Temperature Compensation with Δ/Σ Normalization

When Δ/Σ method is used to extract rotation data reflective and transmissive measuring configuration differ in that the reflective configuration requires only compensation for temperature dependence of the Verdet constant whereas

transmissive configuration require compensation for both Verdet constant and optical activity temperature effects.

8.3.1. Compensation in a reflective configuration

With reflective compensation optical activity cancels out and result of measurement can be expressed as

$$R_R\left(B,\vartheta,T\right)=\frac{1}{4V(T,\vartheta)l(T)}\arcsin\frac{U_1(B)\,\Delta U_2(B)}{U_1(B)\,\Sigma U_2(B)}\ [T]\qquad(8.15)$$

Reflective configuration has therefore no use of the optical activity vs. temperature function. It could be possible to detect the temperature of the crystal by wavelength multiplexing, i.e. by illuminating the crystal at λ_1 and taking the result R_1. At the later instance, the crystal shall be illuminated by another wavelength λ_2 that provides measurement result R_2. Assuming that the wavelength switching is fast enough to presume that the magnetic field and temperature cannot change appreciably one can write

$$
\begin{aligned}
R_1\left(B,\vartheta_1,T\right)&=\frac{1}{4V_1(T,\vartheta_1)l(T)}\arcsin\frac{U_{11}(B)\,\Delta U_{12}(B)}{U_{11}(B)\,\Sigma U_{12}(B)}\ ,\\[2mm]
R_2\left(B,\vartheta_2,T\right)&=\frac{1}{4V_2(T,\vartheta_2)l(T)}\arcsin\frac{U_{21}(B)\,\Delta U_{22}(B)}{U_{21}(B)\,\Sigma U_{22}(B)}
\end{aligned}
\qquad(8.16)
$$

Since arguments of arcsin functions are known from measurements using Δ/Σ normalization it is possible to eliminate magnetic field and crystal length from measurement by dividing the results

$$R_{12}=\frac{R_1\left(B,\vartheta_1,T\right)}{R_2\left(B,\vartheta_2,T\right)}=\frac{V_2(T,\vartheta_2)}{V_1(T,\vartheta_1)}\cdot\frac{\arcsin\dfrac{U_{21}(B)\,\Delta U_{22}(B)}{U_{21}(B)\,\Sigma U_{22}(B)}}{\arcsin\dfrac{U_{21}(B)\,\Delta U_{22}(B)}{U_{21}(B)\,\Sigma U_{22}(B)}}\qquad(8.17)$$

From Eq. (8.17) it is possible to determine the crystal temperature T by finding the temperature where ratio of the Verdet constants equals R_{12}. This is of course possible only if Verdet constants exhibit different $\frac{\partial}{\partial}$ change values. For BiGeO crystal this at red and green wavelengths this is not the case, and therefore this way of determining the crystal temperature is not applicable.

8.3.2. Compensation in a transmissive configuration

For a transmissive configuration one can write

$$R\{B,\},T\} = R_B\{B,\},T\} + R_0\},T\} = \frac{1}{2V(T,\})l(T)} \arcsin \frac{U_1(B) - U_2(B)}{U_1(B) + U_2(B)} \quad [T] \qquad (8.18)$$

With R_B denoting result due to magnetic field and R_0 result due to optical activity. R_0 is a nuisance causing a DC measurement offset that masks the measurement of the DC component of the B. With proper calibration it is possible to set R_0 to zero under $B=0$ condition, *i.e.* no field and at a known temperature. Thus when temperature changes R_0 will shift allowing for determination of the temperature using graphs of optical activity change with temperature. Where only AC magnetic field is measured, this case actually reduces to a case similar to reflective configuration albeit with a half the scale. A temperature compensation for this case using this method has been verified in [27].

For a Δ/Σ method one can therefore conclude that only transmissive configuration can be used if temperature compensation is required.

9.   Conclusion

After the crystal samples were exposed to a femtosecond laser irradiation of increasing power the changes in optical properties of $Bi_{12} Ge O_{20}$ single crystals were observed[1]. The transmittance dependence on the applied irradiation power undergoes initial growth, reaches maximum, and then decreases. The maximal transmittance of 25.1% occurred at 455 mW. In the transmission spectra of unirradiated sample anisotropy was detected see Figure 44. After irradiation, the transmission increased, whereas the anisotropy disappeared. To the best of our knowledge, photo-induced increase in BGO transmission has not been reported before. The XRD measurements performed on the prismatic crystal samples as well as on the powdered slices taken from the crystal facets confirmed mechanical imperfections as well as femtosecond laser induced structural changes. The laser-beam-incident side of the sample became almost amorphous, indicating fragmentation of a mono crystal into disoriented fractals, whereas the side of the crystal sample that was not incident with regard to the laser beam, can be indexed to the $Bi_{12} Ge O_{20}$ compound. The Raman spectra peaks became somewhat stronger, except for the E type peaks at 234, 454, and 619.6 cm^{-1} (Figure 46), which disappeared[1]. Irradiation also caused significant change of the crystal color as shown in Figure 45. The irradiation caused 41.4% decrease in the absorption coefficient and did not influence the Faraday constant. Consequently, the increase in crystal transparency resulted in a significant 70% increase in the magneto-optical quality as shown in Table 6. Optical properties of $Bi_{12} Ge O_{20}$ single crystals can be improved by irradiation with the femtosecond pulsed laser beam. For the best results, the wavelength, duration, and power of irradiating laser beam, need to be optimized.

In order to measure the temperature dependence of the optical activity and Verdet constant of the BiGeO crystal special setups have been created optimized for the measurement. Transmissive configuration was used to measure optical activity and reflective configuration has been used to measure Verdet constant,

since optical activity cancels out in this configuration. An experimental setup was constructed using calibrated Helmholtz coils that were tested for magnetic field uniformity. Measurement of the crystal temperature was a particular problem requiring non-contact measurement due to the sensitivity of the material and possible field disturbance. It was decided to measure the temperature using a radiation thermometer to constantly monitor the crystal. This thermometer was calibrated using a high-performance FLIR IR camera and a material with known emissivity value. Crystal was preheated with a hot gun to a temperature above 100°C and left to cool down while the measurements of optical activity or Verdet constant were taken. Effect of the temperature on optical activity of the BiGeO crystal has been experimentally recorded for two wavelengths, red and green lasing colors. Results of the measurements demonstrate that bot optical activity and Verdet constant are temperature dependent with negative first derivative. Optical activity was also measured on the third wavelength (yellow) for verification purposes. Optical activity vs. temperature curves show that different wavelength exhibit different slope with temperature change. As for Verdet constant, the slopes are very similar but the values of *V* are different - they depend on the wavelength as is known from earlier work. A discussion of temperature effect on both transmissive and reflective Faraday sensor design has been undertaken as well as for two normalization methods. Analysis show that different approaches need to be taken for temperature compensation. It turns out that transmissive configuration offers greatest possibility for determining the crystal temperature using two wavelengths (multi-color measurement).

LIST OF PUBLICATIONS:

Journal articles:

1. Aleksander Kovacevic, Jasna L. Ristic-Djurovic, Marina Lekic, Branka Hadzic, Giuma Saleh Isa Abudagel, Slobodan Petricevic, Pedja Mihailovic, Branko Matovic, Dragan Dramlic, Ljiljana M. Brajovic, Nebojša Romcevic "Influence of femtosecond pulsed laser irradiation on bismuth germanium oxide single crystal properties", Materials Research Bulletin 83 (2016), pp. 284–289, doi: http://dx.doi.org/10.1016/j.materresbull.2016.06.023

2. G. S. I. Abudagel, S. Petricevic, P. Mihailovic, A. Kovacevic, J. L. Ristic-Djurovic, M. Lekic, M. Romcevic, S. irkovic, J. Trajic, N. Romcevic "Improvement of magneto-optical quality of high purity $Bi_{12}GeO_{20}$ single crystal induced by femtosecond pulsed laser irradiation, Optoelectronics and Advanced Materials", Rapid Communications Vol. 11, No. 7-8, July-August 2017, pp. 477 – 481.

Conferences proceedings:

1. Giuma Saleh Isa Abudagel, Slobodan Petri evi , Pedja Mihailovi , Aleksander Kova evi , Jasna L. Risti -Djurovi , Marina Leki , Branka Hadži , Nebojša Rom evi , "Changes of High Purity Bi12GeO20 Single Crystal Properties Induced by Femtosecond Pulsed Laser Irradiation – Serbian Ceramic Society Conference, Serbia, Belgrade, 21st-23rd September 2016, p.73.

10. References

[1] A. Kovačević *et al.*, "Influence of femtosecond pulsed laser irradiation on bismuth germanium oxide single crystal properties," *Mater. Res. Bull.*, vol. 83, pp. 284–289, 2016.

[2] G. S. I. Abudagel *et al.*, "Improvement of magneto-optical quality of high purity Bi12GeO20 single crystal induced by femtosecond pulsed laser irradiation," *Optoelectronics and Advanced Materials, Rapid Communications*, vol. 11, no. 7–8. 2017.

[3] H. Wang, G. Zhang, Z. Guo, J. Wang, and X. Cai, "Application of Electronic Transformers in Digital Substation," in *2008 Joint International Conference on Power System Technology and IEEE Power India Conference*, 2008, pp. 1–5.

[4] G. Frosio and R. Dändliker, "Reciprocal reflection interferometer for a fiber-optic Faraday current sensor.," *Appl. Opt.*, vol. 33, no. 25, pp. 6111–22, 1994.

[5] S. C. Bartlett, F. Farahi, and D. A. Jackson, "Current sensing using Faraday rotation and a common path optical fiber heterodyne interferometer," *Rev. Sci. Instrum.*, vol. 61, no. 9, pp. 2433–2435, 1990.

[6] F. Y. C. Leung, M. S. Demokan, H. K. Government, and H. Kong, "Fiber-optic Current Sensor Developed for Power System Measurement," no. November. pp. 637–643, 1991.

[7] A. Cruden, J. R. McDonald, I. Andonovic, and D. Uttamchandani, "a Magneto-Optic Crystal Based Current Measurement Device," *International Conference on Advances in Power System Control, Operation and Management*. pp. 725–728, 1993.

[8] E. A. Ulmer, "A high-accuracy optical current transducer for electric power systems," *IEEE Trans. Power Deliv.*, vol. 5, no. 2, pp. 892–898, Apr. 1990.

[9] S. H. Zaidi and R. P. Tatam, "Faraday-effect magnetometry: Compensation for the temperature-dependent Verdet constant," *Meas. Sci. Technol.*, vol. 5, no. 12, pp. 1471–1479, 1994.

[10] K. Bohnert, P. Gabus, J. Nehring, and H. Brändle, "Temperature and vibration insensitive fiber-optic current sensor," *J. Light. Technol.*, vol. 20, no. 2, pp. 267–276, 2002.

[11] A. J. Rogers, J. Xu, and J. Yao, "Vibration Immunity for Optical-Fiber Current Measurement," *J. Light. Technol.*, vol. 13, no. 7, pp. 1371–1377, 1995.

[12] K. Turvey, "Determination of Verdet constant from combined ac and dc measurements," *Rev. Sci. Instrum.*, vol. 64, no. 6, pp. 1561–1568, 1993.

[13] A. Jain, J. Kumar, F. Zhou, L. Li, and S. Tripathy, "A simple experiment for determining Verdet constants using alternating current magnetic fields," *Am. J. Phys.*, vol. 67, no. 8, pp. 714–717, 1999.

[14] W. Brandon, S. Mandjiny, K. McDonald, S. Huneycutt, and D. Lee, "High Precision Measurements Lend No Supporting Evidence of Previously Reported Large Verdet Constants for Olive Oil," *Eur. Sci. J.*, no. September, pp. 7–8, 2017.

[15] C. Li, N. Song, and C. Zhang, "Verdet constant measurements of β-barium borate and lead molybdate crystals," *Opt. Mater. Express*, vol. 5, no. 9, p. 1991, 2015.

[16] O. N. D. Ř. E. J. S. Lezák, R. Y. O. Y. Asuhara, A. N. L. Ucianetti, and T. O. M. Ocek, "Temperature-wavelength dependence of terbium gallium garnet ceramics Verdet constant," vol. 6, no. 11, pp. 38–42, 2016.

[17] R. Yasuhara, S. Tokita, J. Kawanaka, and H. Yagi, "Temperature dependence of the Faraday rotation of terbium gallium garnet ceramic," *Ile.Osaka-U.Ac.Jp*.

[18] N. P. Barnes and L. B. Petway, "Variation of the Verdet constant with temperature of terbium gallium garnet," *Journal of the Optical Society of America B*, vol. 9, no. 10. p. 1912, 1992.

[19] V. Antonov, B. Harmon, and a Yaresko, *Electronic structure and magneto-optical properties of solids*. 2004.

[20] T. Oakberg, "Magneto-optic Kerr effect," *HINDS Instruments*, pp. 1–6, 2005.

[21] B. E. A. Saleh and M. C. Teich, *Fundamentals of Photonics*. New York, USA:

John Wiley & Sons, Inc., 1991.

[22] Z. Ž. Lazarević *et al.*, "Determination of magneto-optical quality and refractive index of bismuth germanium oxide single crystals grown by Czochralski technique," *Opt. Mater. (Amst).*, vol. 34, no. 11, pp. 1849–1859, 2012.

[23] Galstyan Ogsen, "Magneto-Optical Thin Films For Magnetic Fields Visualization", PhD Thesis, 2105.

[24] S. Wittekoek, T. J. A. Popma, J. M. Robertson, and P. F. Bongers, "Magneto-optic spectra and the dielectric tensor elements of bismuth-substituted iron garnets at photon energies between 2.2-5.2 eV," *Phys. Rev. B*, vol. 12, no. 7, pp. 2777–2788, 1975.

[25] D. R. Tobergte and S. Curtis, *Crystals and crystal structures*, vol. 53, no. 9. 2013.

[26] J. Kobayashi, T. Takahashi, T. Hosokawa, and Y. Uesu, "A new method for measuring the optical activity of crystals and the optical activity of KH_2PO_4," *J. Appl. Phys.*, vol. 49, no. 2, pp. 809–815, 1978.

[27] P. M. Mihailovic, S. J. Petricevic, and J. B. Radunovic, "Compensation for temperature-dependence of the faraday effect by optical activity temperature shift," *IEEE Sens. J.*, vol. 13, no. 2, pp. 832–837, 2013.

[28] J. W. P. Peatross, "Physics of Light and Optics," pp. 1–341, 2008.

[29] T. Johansson, P. Jensen, and C. Krag, "Helmholtz coils for characterization of magentic sensors," 2003.

[30] P. D. P. M. Mihailovi, P. D. S. J. Petricevi, P. D. Z. M. Stevi, and P. D. J. B. Radunovi, "Normalization And Temperature Compensation For Extrinsic Fiber-Optic Sensors," pp. 94–97, 2013.

[31] Raytek, "Principles of Non-contact Temperature Measurement," *J. Sol. Energy Eng.*, vol. 3, no. February, p. 1397, 2003.

[32] U. S. Karl Ehinger, Dieter Flach, Lothar Gellrich Eberhard Horlebein, Dr. Ralf Huck Henning Ilgner, Thomas Kayser Harald Müller, Helga Schädlich Andreas Schüssler, "Industrial temperature measurement Basics and

practice," pp. 1–203, 2013.

[33] J. Point and T. Measurements, "Infrared Thermometers Just Point and Shoot for Quality Noncontact Temperature Measurements."

[34] S. Model *et al.*, "GLM – series," pp. 43–44.

[35] W. I. Madden, W. C. Michie, A. Cruden, P. Niewczas, J. R. McDonald, and I. Andonovic, "Temperature compensation for optical current sensors," *Opt. Eng.*, vol. 38, no. 10, p. 1699, 1999.

[36] A. Kovačević *et al.*, "Influence of femtosecond pulsed laser irradiation on bismuth germanium oxide single crystal properties," *Mater. Res. Bull.*, vol. 83, 2016.

[37] T. Haider, "A Review of Magneto-Optic Effects and Its Application," *Int. J. Electromagn. Appl.*, vol. 7, no. 1, pp. 17–24, 2017.

[38] F. L. P. and P. Bandettini, "Faraday Rotation in Undergraduate Advanced Laboratory," *Am. J. Phys*, vol. 58 (6), p. 542, 1990.

[39] et al Y. Ruan, "No Title," *Opt. Commun.*, vol. 39, p. 252, 2005.

[40] G. H. Dieke and R. A. Satten, "Spectra and Energy Levels of Rare Earth Ions in Crystals," *Am. J. Phys.*, vol. 38, no. 3, pp. 399–400, 1970.

[41] G. H. Dieke and R. A. Satten, "Spectra and Energy Levels of Rare Earth Ions in Crystals," *Am. J. Phys.*, vol. 38, no. 3, pp. 399–400, 1970.

[42] "PDXL Version 2.0.3.0 Integrated X-ray Powder Diffraction Software. Rigaku Corporation, Tokyo, Japan, 2011, pp. 196–8666." Corporation, Tokyo, Japan, 2011, pp. 196–8666.

11. Appendix

MatLab Code

```
1 %------------------------------------------------------------------------------------------
2 % Filename: magfel.m
3 % This program calculates the magnetic field along the z axis of a set of
4 % Helmholtz coils, where the two coils are connected in series, all size s are
5 %   given in SI units.
6 %------------------------------------------------------------------------------------------
7 % Diameter of the wire (including insulation)
8 % d =2* 10^ ( -3);
9 %------------------------------------------------------------------------------------------
10 % Current running through the wire
11 % I =4.14;
12 %------------------------------------------------------------------------------------------
13 % Radius of the coils (distance from the center to the beginning of the first
14 % winding)
15 % R-0=0.115;
16 %------------------------------------------------------------------------------------------
17 % Width of each of the coils
18 % a= 17*d
19 %------------------------------------------------------------------------------------------
20 % Height of each of the coils
21 % b=d+3 3*sqrt (3)/2 *d
22 %------------------------------------------------------------------------------------------
23 % Permeability of the vacuum
24 % mu-v= 0= 4*pi*10-(- 7);
25 %------------------------------------------------------------------------------------------
26 % Number of windings in the width (in the first layer)
27% N- j= a/ d
28 %------------------------------------------------------------------------------------------
```

29 % Number of windings in the height

30 % N-i= (b-d)/(sqrt (3) /2*d) + 1

31 %---

32 % N- j - 1/2 is the average number of windings in the width and

33% rem (N-i ,2) compensates if N-i is an odd number

34 % total number of winding s=N-i* (N-j -1/2) +1/2 *r e m (N-i, 2)

35 %---

36 % x position of the first winding

37 % x1= R-0+d/2;

38 %---

39 % z position of the first winding

40 % z1 =0.089/2+d / 2 ;

41 %---

42 % Initializes a parameter used later

43 % k start =1;

44 %---

45 %Sets the z values for which the B field is calculated for

46 %for z=linspace (-0.15,0.15,100)

47 %---

48 % Initializes parameters used later

49 %---

50   B-1ofz-start = 0;

51   B-2ofz-start = 0;

52 %---

53 % Loop that runs through all the layers with the number of N-j wires in

54 %   them. I t sums up each of these wire's contribution to the magnetic field.

55 %   for j =1: N-j

56 %---

57 %   for i =1:2: N-i

58 %   x-i= x1 + (i-1)*sqrt (3) / 2* d;

```
59 %-------------------------------------------------------------------------------------
60 %            z-j= z1 + ( j-1)* d;
61 %-------------------------------------------------------------------------------------
62 %            B-1ofz=B-1ofz-start + (mu-v*I _ x i^2)/2_((( x-i)^2+( z-z-j)^2 )^
63 %                 (-3/2)+ (( x i)^2+( z +z- j) ^ 2 ) ^ ( -3/2) ) ;
64 %-------------------------------------------------------------------------------------
65 %             B-1ofz-start=B-1ofz ;
66 %-------------------------------------------------------------------------------------
67           end
68 %-------------------------------------------------------------------------------------
69 %       end
70 %-------------------------------------------------------------------------------------
71%   Loop that runs through al l the layers with the number of N-j -1 wires in
72 %   them .I t sums up each of these wire ' s contribution to the magnetic
73 % field.
74 %       for j =1: N j  1
75 %-------------------------------------------------------------------------------------
76 %          for i-2:2: N-i
77 %-------------------------------------------------------------------------------------
78 %          x-i= x1 + ( i-1)_sqrt (3)/2*d;
79 %-------------------------------------------------------------------------------------
80 %          z-j=-z1+d/2 + (j-1)* d;
81 %-------------------------------------------------------------------------------------
82 %          B-2ofz=B-2iofz-start + ( mu-v*I * x- i^2) /2_((( x-i)^2 + ( z  z-j ) ^2)
83 %         ^(-3/2) + ( x-i ) ^2+(z+ z-j ) ^2) ^ (-3/2) ) ;
84 %-------------------------------------------------------------------------------------
85 %          B-2ofz-start=B-2ofz;
86 %-------------------------------------------------------------------------------------
87 %          end
88 %-------------------------------------------------------------------------------------
```

```
89 %          end
90 %---------------------------------------------------------------------------------------
91 %    k=k-start;
92 %---------------------------------------------------------------------------------------
93 % Adds the contributions from the layers with N-j wires and N-j-1 wires.
94 % This gives the total magnetic field of the Helmholtz coil s as a function
95 %o f the distance along the z-axis.
96 %       B(k) = B-1ofz+B-2ofz ;
97 %---------------------------------------------------------------------------------------
98       k-start-k +1;
99 %---------------------------------------------------------------------------------------
100   end
101 %---------------------------------------------------------------------------------------
102 % Plots B as a function of z, where z is normalized in orders of the average
103 % radius (t h e distance from the center of the coil to the middle of the
104 % windings). The average radius is also the distance between the two coils.
105 %    close all
106 %    z=linspace (- 0.15/0.113,0.15/0.113,100);
107 %    plot (z , B )
108 %    grid on
109 %  xlabel (' z/R –{av} ')
110 %    ylabel (' B [T] ')
```

Biography

Personal Data
Name: Giuma Saleh Isa
Surname: Abudagel
Nationality: Libyan
Date of Birth: 01.01.1963
Specialization: Optoelectronics and Laser Technology
Scientific Degree: Assistant Professor
Job Place: Physics Dept- Faculty of Science- Azzaytuna University- Libya
E Mail: giuma05@yahoo.com
Tel: +381612774249
Tel: +218925614249

Scientific Qualification:
1987- B. SC in Physics from Department of Physics, Faculty of Science, University of Tripoli, Tripoli Libya.
2000- M. SC in Optoelectronics and Laser technology from Faculty of Electrical Engineering, University of Belgrade, Serbia.
From Feb 2014 until now, Doctoral student at Faculty of Electrical Engineering, University of Belgrade, Serbia.

Academic Appointments & Work experience:
1989-2008: full time Researcher in Laser & optics at Central Agency for Research and Manufacturing, Tripoli Libya.
2000-2005: half time lecturer of theoretical and experimental physics for undergraduate students Department of Physics, Faculty of Science, University of Tripoli.
2008-2013: full time lecturer of theoretical and experimental physics for undergraduate students, Azzaytuna University Libya.

Прилог 1.

Изјава о ауторству

Потписани-а *Giuma Saleh Isa Abudagel*

број уписа *2013/5053*

Изјављујем

да је докторска дисертација под насловом

Experimental characterization of Magneto optical Properties of Faraday Crystal Applied In Magnetic Field Sensor

- резултат сопственог истраживачког рада,
- да предложена дисертација у целини ни у деловима није била предложена за добијање било које дипломе према студијским програмима других високошколских установа,
- да су резултати коректно наведени и
- да нисам кршио/ла ауторска права и користио интелектуалну својину других лица.

Потпис докторанда

У Београду, *12/10/2018*

Прилог 2.

Изјава о истоветности штампане и електронске верзије докторског рада

Име и презиме аутора _Giuma Saleh Isa Abudagel_

Број уписа _2013/5053_

Студијски програм _NANOELEKTRONIKA i FOTONIKA_

Наслов рада _Experimental characterization of magneto optical Properties of Faraday crystal Apllied_

Ментор _Slobodan Petricevic in magnetic field sensor_

Потписани _Giuma Saleh Isa Abudagel_

изјављујем да је штампана верзија мог докторског рада истоветна електронској верзији коју сам предао/ла за објављивање на порталу Дигиталног репозиторијума Универзитета у Београду.

Дозвољавам да се објаве моји лични подаци везани за добијање академског звања доктора наука, као што су име и презиме, година и место рођења и датум одбране рада.

Ови лични подаци могу се објавити на мрежним страницама дигиталне библиотеке, у електронском каталогу и у публикацијама Универзитета у Београду.

Потпис докторанда

У Београду, _12/10/2018_

Прилог 3.

Изјава о коришћењу

Овлашћујем Универзитетску библиотеку „Светозар Марковић" да у Дигитални репозиторијум Универзитета у Београду унесе моју докторску дисертацију под насловом:

Experimental characterization of magneto optical Properties of Faraday crystal Applied in magnetic field sensor

која је моје ауторско дело.

Дисертацију са свим прилозима предао/ла сам у електронском формату погодном за трајно архивирање.

Моју докторску дисертацију похрањену у Дигитални репозиторијум Универзитета у Београду могу да користе сви који поштују одредбе садржане у одабраном типу лиценце Креативне заједнице (Creative Commons) за коју сам се одлучио/ла.

1. Ауторство

(2.) Ауторство - некомерцијално

3. Ауторство – некомерцијално – без прераде

4. Ауторство – некомерцијално – делити под истим условима

5. Ауторство – без прераде

6. Ауторство – делити под истим условима

(Молимо да заокружите само једну од шест понуђених лиценци, кратак опис лиценци дат је на полеђини листа).

Потпис докторанда

У Београду, 12 /10 / 2018

1. Ауторство - Дозвољавате умножавање, дистрибуцију и јавно саопштавање дела, и прераде, ако се наведе име аутора на начин одређен од стране аутора или даваоца лиценце, чак и у комерцијалне сврхе. Ово је најслободнија од свих лиценци.

2. Ауторство – некомерцијално. Дозвољавате умножавање, дистрибуцију и јавно саопштавање дела, и прераде, ако се наведе име аутора на начин одређен од стране аутора или даваоца лиценце. Ова лиценца не дозвољава комерцијалну употребу дела.

3. Ауторство - некомерцијално – без прераде. Дозвољавате умножавање, дистрибуцију и јавно саопштавање дела, без промена, преобликовања или употребе дела у свом делу, ако се наведе име аутора на начин одређен од стране аутора или даваоца лиценце. Ова лиценца не дозвољава комерцијалну употребу дела. У односу на све остале лиценце, овом лиценцом се ограничава највећи обим права коришћења дела.

4. Ауторство - некомерцијално – делити под истим условима. Дозвољавате умножавање, дистрибуцију и јавно саопштавање дела, и прераде, ако се наведе име аутора на начин одређен од стране аутора или даваоца лиценце и ако се прерада дистрибуира под истим или сличном лиценцом. Ова лиценца не дозвољава комерцијалну употребу дела и прерада.

5. Ауторство – без прераде. Дозвољавате умножавање, дистрибуцију и јавно саопштавање дела, без промена, преобликовања или употребе дела у свом делу, ако се наведе име аутора на начин одређен од стране аутора или даваоца лиценце. Ова лиценца дозвољава комерцијалну употребу дела.

6. Ауторство - делити под истим условима. Дозвољавате умножавање, дистрибуцију и јавно саопштавање дела, и прераде, ако се наведе име аутора на начин одређен од стране аутора или даваоца лиценце и ако се прерада дистрибуира под истим или сличном лиценцом. Ова лиценца дозвољава комерцијалну употребу дела и прерада. Слична је софтверским лиценцама, односно лиценцама отвореног кода.